



Contents lists available at ScienceDirect

European Journal of Medicinal Chemistry

journal homepage: <http://www.elsevier.com/locate/ejmech>

Research paper

## Discovery of novel CA-4 analogs as dual inhibitors of tubulin polymerization and PD-1/PD-L1 interaction for cancer treatment

Xuchao Yang<sup>a,1</sup>, Binbin Cheng<sup>a,1</sup>, Yao Xiao<sup>b,1</sup>, Mingming Xue<sup>c</sup>, Ting Liu<sup>a</sup>, Hao Cao<sup>a</sup>, Jianjun Chen<sup>a,\*</sup>

<sup>a</sup> School of Pharmaceutical Sciences, Guangdong Provincial Key Laboratory of New Drug Screening, Southern Medical University, Guangzhou, 510515, China

<sup>b</sup> Wuhan Wuchang Hospital, Wuchang Hospital Affiliated to Wuhan University of Science and Technology, 430063, China

<sup>c</sup> Tianjin Tiancheng Chemical Co., Ltd., Chemical Street, Binhai New District, Tianjin, 300480, China

## ARTICLE INFO

## Article history:

Received 25 September 2020

Received in revised form

11 November 2020

Accepted 24 November 2020

Available online xxx

## Keywords:

Tubulin polymerization

PD-L1 inhibitor

Immunotherapy

## ABSTRACT

A series of novel CA-4 analogs as dual inhibitors of tubulin polymerization and PD-1/PD-L1 were designed, synthesized and bio-evaluated. Among them, compound TP5 exhibited strongest inhibitory effects against five cancer cell lines with an IC<sub>50</sub> value of 800 nM in HepG2 cells. In addition, mechanism studies revealed that TP5 could effectively inhibit tubulin polymerization, suppress HepG2 cells migration and colony formation, and cause cell arrest at G2/M phase and induce apoptosis. Furthermore, TP5 exhibited moderate anti-PD-1/PD-L1 activity with IC<sub>50</sub> values of 48.76 μM in a homogenous time-resolved fluorescence (HTRF) assay. *In vivo* efficacy studies indicated that TP5 could significantly suppress tumor growth in an immune checkpoint humanized mouse model with a Tumor Growth Suppression (TGI) of 57.9% at 100 mg/kg without causing significant toxicity. Moreover, TP5 did not cause *in vivo* cardiotoxicity in BALB/c mice. These results suggest that the novel CA-4 analogs may serve as a starting point for developing more potent dual inhibitors of tubulin polymerization and PD-1/PD-L1.

© 2020 Elsevier Masson SAS. All rights reserved.

## 1. Introduction

Cancer has become the second leading cause of death and a major public health problem globally [1]. Current molecularly targeted therapies aim to bind selectively to a single biological entity (e.g. a protein) to avoid unwanted off-target effects. However, cancer is a complex disease with multiple signaling pathways dysregulated, therefore, single-target drugs cannot adequately achieve therapeutic effects. This provoked the search for therapeutics with multi-targeting capabilities [2]. Compared with single-target drugs, multi-target therapeutics can act on more than one target, thus achieve greater efficacy and are less vulnerable to drug resistance [3,4].

Recent studies showed that the combination of anti-PD-1/PD-L1 antibodies and cytotoxic agents (e.g. tubulin inhibitors: paclitaxel

and BNC105) can achieve synergistic effects and better antitumor efficacy, and that the combination therapy could be safer than chemotherapeutic agents alone [5–8]. However, combination therapy has several drawbacks including unpredictable pharmacokinetics (PK) and pharmacodynamics (PD) with a mixture of two or more drugs. An alternative approach is to design a single molecule with the capability to act on multiple validated cancer drug targets. It is relatively easy to predict the PK and PD of a single molecule. In addition, single molecules are more amenable to structural modifications which offers the added advantage of performing structure–activity relationship studies more rapidly.

We have previously described the discovery of several classes of Combretastatin A-4 (CA-4)-based tubulin inhibitors [9,10] and resorcinol dibenzyl ether-based PD-1/PD-L1 inhibitors [11,12], which showed potent anticancer activities *in vitro* and *in vivo*. Microtubules play a key role in the division and proliferation of tumor cells, and have been targeted by many anti-tumor drugs such as taxanes and vinca alkaloids [13]. CA-4, as a representative tubulin inhibitor binding at the colchicine site, exhibits potent antitumor activities in various cancer cell lines [14]. However, the further development of CA-4 was hindered by the poor water solubility, toxic side effects and P-gp mediated multi-drug resistance (MDR)

**Abbreviations:** PD-1, programmed cell death-1; PD-L1, programmed cell death-ligand 1; FCM, flow cytometry; H&E, haematoxylin and eosin; TGI, Tumor Growth Inhibition; HTRF, homogenous time-resolved fluorescence.

\* Corresponding author.

E-mail address: [jchen21@smu.edu.cn](mailto:jchen21@smu.edu.cn) (J. Chen).

<sup>1</sup> These authors contributed equally.

<https://doi.org/10.1016/j.ejmech.2020.113058>

0223-5234/© 2020 Elsevier Masson SAS. All rights reserved.

[15]. As for cancer immunotherapy, it is one of the most actively pursued areas in anticancer drug discovery because of its high selectivity and low toxicity [16]. Currently, PD-1/PD-L1 is one of the most promising targets in the field of immuno-oncology [17]. In the past decades, numerous PD-1/PD-L1 inhibitors have been discovered, including small molecules, peptidomimetics, and monoclonal antibodies [18,19].

We carefully analyzed the pharmacophores of the small molecule PD-1/PD-L1 inhibitor BMS-200 and the tubulin inhibitor CA-4, with four pharmacophoric points (core group, linker, aryl group and tail group) identified for the PD-1/PD-L1 inhibitors (Fig. 1) [11,12,20,21]. We found that CA-4 and the core group (red colored structural moieties in Fig. 1) of BMS-200 have similar physicochemical properties (e.g. Log P and tPSA), and that large substitutions on the hydroxyl group of CA-4 is tolerable based on the docking analysis [10], this inspired us to design dual inhibitors of tubulin and PD-1/PD-L1 through a hybridization strategy. With this in mind, we designed, synthesized and bio-evaluated 20 novel CA-4 analogs as dual-acting tubulin and PD-1/PD-L1 inhibitors. Among them, compound TP5 displayed high anti-proliferative potency against a panel of cancer cell lines as well as moderate anti-PD-1/PD-L1 activity, making it a promising lead compound for future development.

## 2. Results and discussion

### 2.1. Chemistry

The synthesis of CA-4 analogs TP1–20 is outlined in Scheme 1. Briefly, the hydroxyl group of 4-(hydroxymethyl)benzaldehyde compound 1 was brominated by tribromoborane to give 4-(bromomethyl)benzaldehyde intermediate M1. Then the benzyl bromide moiety of intermediate M1 was reacted with the hydroxyl group of CA-4 to yield the benzylated CA-4 analog M2. Finally, the NaBH<sub>3</sub>CN-mediated reductive amination was applied to convert M2 and various amines to the desired compounds TP1–20 according to a known procedure [22].

Reagents and conditions: (a) BBr<sub>3</sub>, THF, 0 °C, 2 h, 80%; (b) DMF, Na<sub>2</sub>CO<sub>3</sub>, 80 °C, 30 min, 60%; (c) DMF, AcOH, NaBH<sub>3</sub>CN, various amines, 80 °C, 2 h, 15%–25%.

**In vitro antiproliferative activity.** The *in vitro* antiproliferative efficacy of these dual-action agents were evaluated against five cancer cell lines (HepG2, MC38, HeLa, B16F10, paclitaxel-resistant A549/PTX) and two non-tumoral cell lines (HEK293 and NCM460), through CCK-8 assay with CA-4 as positive control. As presented in Table 1, most of the CA-4 analogs displayed moderate to high antiproliferative activities with IC<sub>50</sub> values in the nanomolar to micromolar range. Among them, TP5 showed the best overall activity with IC<sub>50</sub> values of 0.8 μM, 0.9 μM, 4.8 μM, and 4.2 μM against HepG2, MC38, HeLa, and B16F10, respectively. Furthermore, TP5 exhibited much higher activity against the paclitaxel-resistant A549/PTX cells with an IC<sub>50</sub> of 1.5 μM, as compared to paclitaxel

which is essentially inactive (IC<sub>50</sub> = 18.9 μM). In addition, TP5 showed negligible cytotoxicity to normal cells (IC<sub>50</sub> > 40 μM for HEK-293 and NCM460), indicating that TP5 was selectively cytotoxic to tumor cells over normal cells. It was worth noting that compounds TP2, TP3, TP5, TP7, TP10, and TP20 bearing a straight tail group displayed stronger antiproliferative effects against cancer cells with IC<sub>50</sub> values ranging from 0.8 μM to 10 μM, as compared to compounds with amino acid tail groups (e.g. pipecolic acid for TP17,TP18; 2,2-dimethyl glycine for TP4) or small rings tail groups (e.g. pyrrolidine for TP12–15; azetidine for TP11), suggesting that amino acid or small ring tail groups are sub-optimal for anti-proliferative activity.

**In vitro tubulin polymerization assay.** To explore the mechanism of action, we conducted a tubulin polymerization assay using several CA-4 derivatives with potent, moderate, mild or no cytotoxic activities at the same concentration. As depicted in Fig. 2, TP5 with potent cytotoxicity exhibited strong inhibitory effects against tubulin polymerization (IC<sub>50</sub> = 16.1 μM), and the activity was significantly better than that of the compounds with moderate antiproliferative activity such as TP2 (IC<sub>50</sub> = 60.7 μM) and TP7 (IC<sub>50</sub> = 201.5 μM). TP5 was also superior to the compounds with mild or no cytotoxicity such as TP15 (IC<sub>50</sub> > 200 μM) and TP17 (IC<sub>50</sub> > 200 μM). Moreover, TP5 inhibited tubulin polymerization in a concentration-dependent manner, which correlated well with its antiproliferative effects. It is also worth noting that CA-4 inhibited tubulin polymerization with an IC<sub>50</sub> value of 4.31 μM, while paclitaxel as a microtubule stabilizer had no depolymerization effect.

**Immunofluorescence staining.** Based on the high *in vitro* antiproliferative and anti-tubulin activity, TP5 was selected to evaluate the inhibitory effects on microtubule dynamics using a HepG2 cell line by immunofluorescence staining. As illustrated in Fig. 3, the microtubule network was obviously destroyed after treatment with TP5 at a concentration of 5 μM, as compared to control experiment, which correlated well with its inhibitory activity against tubulin polymerization.

**Inhibition of cancer cells migration and colony formation.** Tumor cells are able to migrate to distant organs, resulting in the formation of metastasized tumors. We have previously shown that microtubule polymerization inhibitors could inhibit cancer cell migration [9]. Therefore, we evaluated the anti-migratory effects of TP5, as well as its ability to inhibit colony formation using HepG2 cells. As shown in Fig. 4A and B, the wound closure was significantly suppressed by TP5, indicating that TP5 could weaken the migratory ability of HepG2 cells. In addition, TP5 also potently inhibited the colony formation of HepG2 cells in a dose-dependent manner (Fig. 4C and D).

**Cell-cycle, apoptosis, and mitochondrial membrane potential (ΔΨ<sub>m</sub>) assay.** To further explore the anticancer mechanism of action of TP5, we evaluated the effects of TP5 on the cell cycle, apoptosis, and ΔΨ<sub>m</sub> of HepG2 cells with flow cytometry and fluorescence analysis. As shown in Fig. 5, treatment with TP5 dose-dependently increased the percentages of cells arrested at G2/M

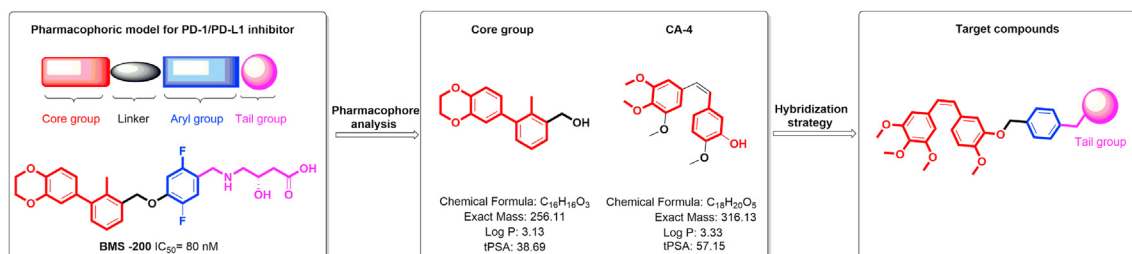
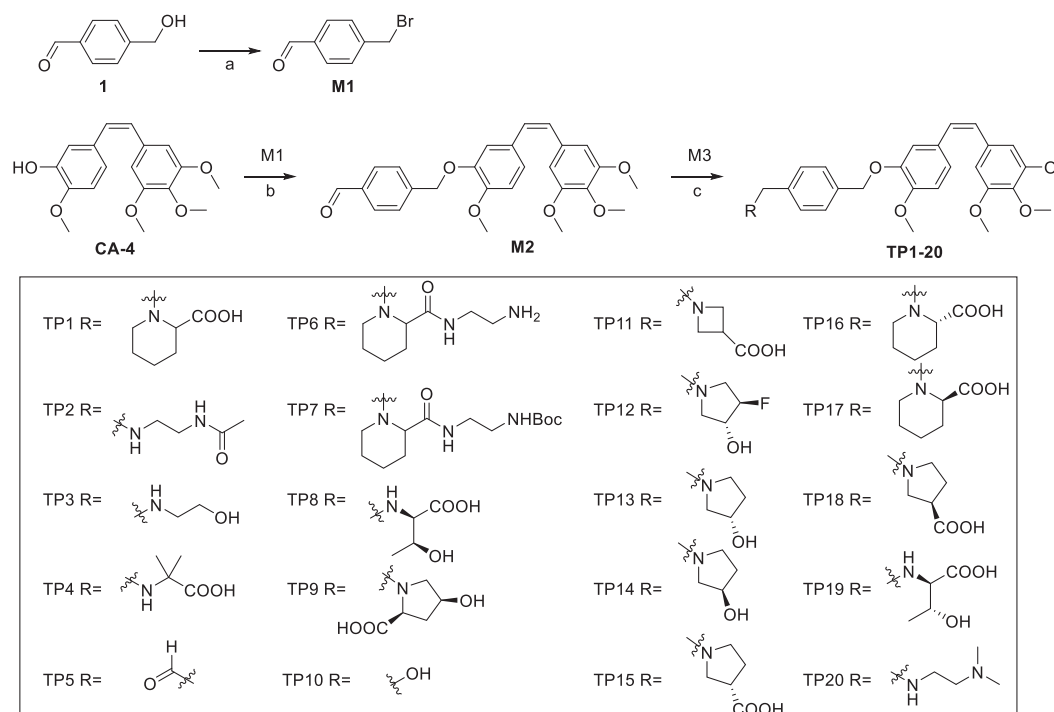


Fig. 1. Design of target compounds based on the pharmacophores of the tubulin inhibitor CA-4 and PD-1/PD-L1 inhibitor BMS-200.

Scheme 1. Synthesis of CA-4 analogs TP1–20<sup>a</sup>

**Table 1**  
In Vitro growth inhibitory effects of the newly synthesized compounds<sup>a</sup>.

ID	Cytotoxic effects: IC <sub>50</sub> (μM)						
	HepG2	MC38	HeLa	B16F10	A549/PTX	HEK293	NCM460
TP1	3.1 ± 0.1	5.4 ± 0.08	14.2 ± 0.7	>10	10.2 ± 0.6	>50	>50
TP2	6.1 ± 0.2	1.8 ± 0.05	6.4 ± 0.1	2.5 ± 0.1	1.1 ± 0.1	>50	54 ± 1.6
TP3	5.9 ± 0.3	1.2 ± 0.04	4.4 ± 0.1	6.6 ± 0.2	0.8 ± 0.02	>50	39 ± 1.3
TP4	6.5 ± 0.4	>10	>10	>10	>20	>50	>50
TP5	0.8 ± 0.02	0.9 ± 0.03	4.8 ± 0.3	4.2 ± 0.4	1.5 ± 0.2	46 ± 1.1	41 ± 1.2
TP6	4.8 ± 0.3	>10	7.3 ± 0.2	4.6 ± 0.2	2.7 ± 0.3	>50	>50
TP7	1.1 ± 0.03	1.9 ± 0.06	2.0 ± 0.1	4.7 ± 0.2	15 ± 1.2	48 ± 1.3	28 ± 1.1
TP8	>10	>10	>10	5.4 ± 0.5	>20	>50	>50
TP9	>10	>10	>10	>10	>20	>50	>50
TP10	2.4 ± 0.5	5.7 ± 0.1	7.6 ± 0.3	6.6 ± 0.3	12 ± 1.3	37 ± 1.4	>50
TP11	>10	>10	6.5 ± 0.1	>10	>20	>50	>50
TP12	5.3 ± 0.1	>10	9.2 ± 0.4	>10	19.2 ± 1.6	29 ± 1.2	38 ± 1.5
TP13	6.2 ± 0.3	6.9 ± 0.3	>10	>10	8.9 ± 0.4	>50	53 ± 1.7
TP14	6.6 ± 0.4	7.2 ± 0.2	10.5 ± 0.6	>10	5.9 ± 0.4	>50	51 ± 1.2
TP15	2.3 ± 0.1	6.3 ± 0.1	12.8 ± 0.3	>10	>20	27 ± 1.5	>50
TP16	>10	>10	>10	>10	>20	42 ± 1.1	>50
TP17	>10	>10	>10	>10	>20	>50	>50
TP18	6.4 ± 0.4	>10	>10	7 ± 0.4	12 ± 0.9	>50	>50
TP19	>10	>10	>10	>10	>20	>50	>50
TP20	4.4 ± 0.1	1.4 ± 0.1	9.4 ± 0.3	>10	1.6 ± 0.2	39 ± 1.2	35 ± 1.1
CA-4	0.59 ± 0.04	0.08 ± 0.003	0.06 ± 0.002	0.05 ± 0.002	0.62 ± 0.05	11 ± 0.3	12 ± 0.4

<sup>a</sup>Cells were treated with different concentrations of synthesized compounds for 48 h. Cell viability was measured by the CCK-8 assay as described in the Experimental Section. The data are generated from three independent experiments.

phase (Fig. 5A). In addition, flow cytometric and fluorescence analysis revealed that Annexin-FITC/PI-positive apoptotic cells were increased dramatically after treatment with TP5 (Fig. 5B and D). Moreover, the  $\Delta\Psi_m$  in HepG2 cells was moderately reduced compared with the control group (Fig. 5C and E).

PD1/PD-L1 binding assay. The activities of CA-4 analogs as inhibitors of the PD-1/PD-L1 interaction were evaluated using the well-established homogenous time-resolved fluorescence (HTRF) assay as described in the Experimental Section. As listed in Table 2, TP2, TP3, TP5, TP6, TP8, TP11, TP12, TP14, TP18, TP19 which bear a

short chain or small rings (e.g. pyrrolidine and azetidine), displayed moderate anti-PD-1/PD-L1 activity with IC<sub>50</sub> values in the mid-micromolar range (38.57–90.55 μM). It is worthy of note that CA-4 was not active at concentrations up to 100 μM.

Molecular docking studies. To gain insights into the interaction of these dual-action conjugates with their target proteins, we conducted molecular modeling studies by docking the most active compound TP5 into tubulin and PD-L1. As shown in Fig. 6A and B, TP5 binds well to the colchicine binding site of tubulin. One hydrogen bond was formed between TP5 and tubulin: the methoxy

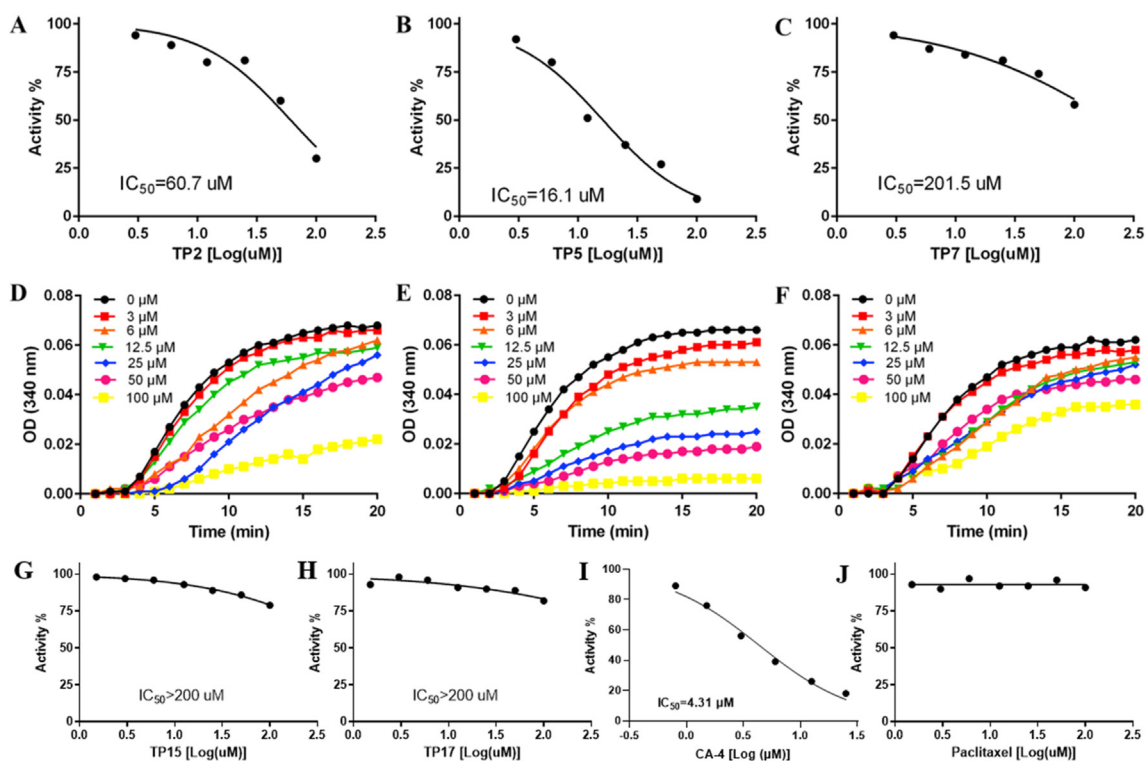


**Fig. 2.** Inhibition of tubulin polymerization by CA-4 derivatives. (A) TP2; (B) TP5; (C) TP7; and dose-dependent inhibition of tubulin polymerization by (D) TP2; (E) TP5; (F) TP7; The inhibition of tubulin polymerization by TP15 (G), TP17 (H), CA-4(I), and Paclitaxel (J).

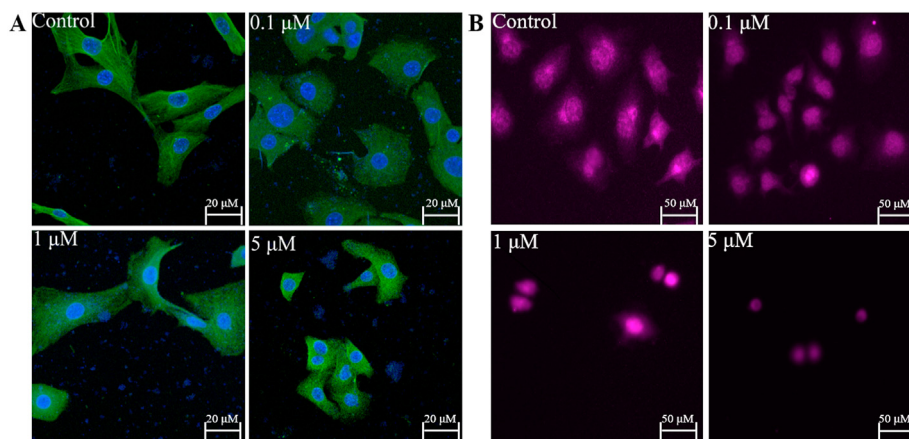


**Fig. 3.** Effects of TP5 on the cellular microtubule networks. HepG2 cells were treated with vehicle control 0.1% DMSO or TP5 for 24 h. (A) Microtubules were visualized with an anti- $\beta$ -tubulin antibody (green); (B) Microtubules were visualized with an anti- $\beta$ -tubulin antibody (red). (For interpretation of the references to color in this figure legend, the reader is referred to the Web version of this article.)

group of the TMP (3,4,5-trimethoxyphenyl) with the  $-C=O$  of VAL236. In addition, TP5 was firmly wrapped in the colchicine-binding site with the formation of a tight hydrophobic “sandwich” by the side-chains of CYS239, ASN247 and ALA248 from one side and that of LYS252 and LEU253 from the other side. As for the binding interactions with PD-L1, Fig. 6C and D revealed that TP5 fitted relatively well into the hydrophobic cleft formed by the dimeric PD-L1, the central phenyl ring moiety of TP5 formed  $\pi$ - $\pi$  interactions with TYR56 of PD-L1, consistent with our previous observations for the binding interaction of similar compounds in the binding interface of dimeric PD-L1 [12].

TP5 demonstrated similar binding affinities to human PD-L1 and

murine PD-L1 *in vitro*. To verify whether the human specific PD-L1 inhibitor TP5 can cross-react with mouse PD-L1, we determined its binding affinity to human PD-L1 (hPD-L1) and mouse PD-L1 (mPD-L1) by using isothermal titration calorimetry (ITC) and surface plasmon resonance (SPR). As shown in Table 3, TP5 exhibited moderate activity with human PD-L1 (ITC:  $K_D = 117 \mu\text{M}$ ; SPR  $K_D = 49.5 \mu\text{M}$ ), which is consistent with the HTRF assay results ( $IC_{50} = 49 \mu\text{M}$ ). Importantly, TP5 showed similar binding affinity for human PD-L1 and mouse PD-L1 (ITC  $K_D$  of  $117 \mu\text{M}$  for hPD-L1 vs  $75.4 \mu\text{M}$  for mPD-L1; SPR  $K_D$  of  $49.5 \mu\text{M}$  for hPD-L1 vs  $112 \mu\text{M}$  for mPD-L1).

Humanized knock-in mouse models for evaluating *in vivo* efficacy

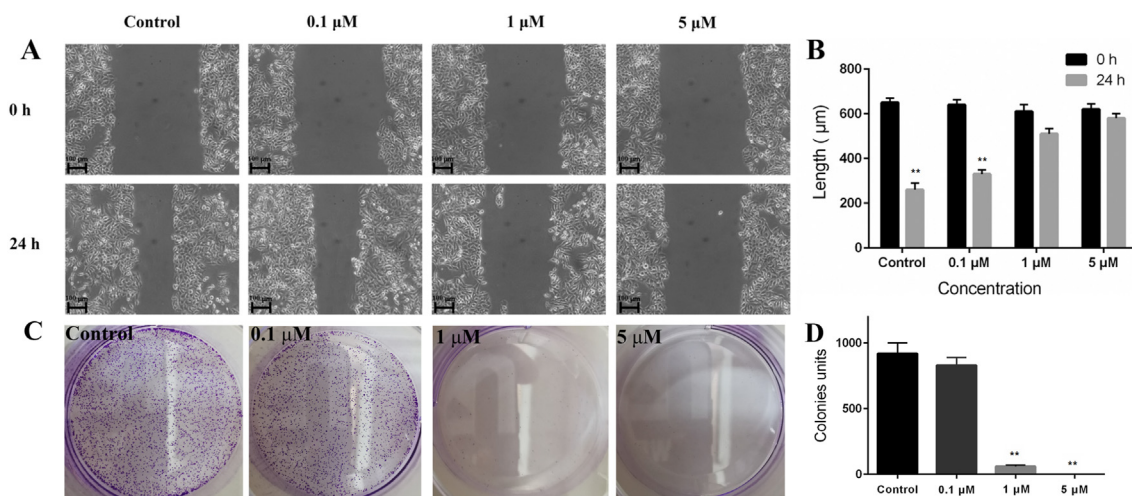


**Fig. 4.** Inhibition of cancer cell migration and colony formation. (A) Effects of TP5 on HepG2 cell migration; (B) Histograms displayed the length of the scratches; (C) Effects of TP5 on colony formation of HepG2 cells; (D) Histograms displayed the number of colonies formed.

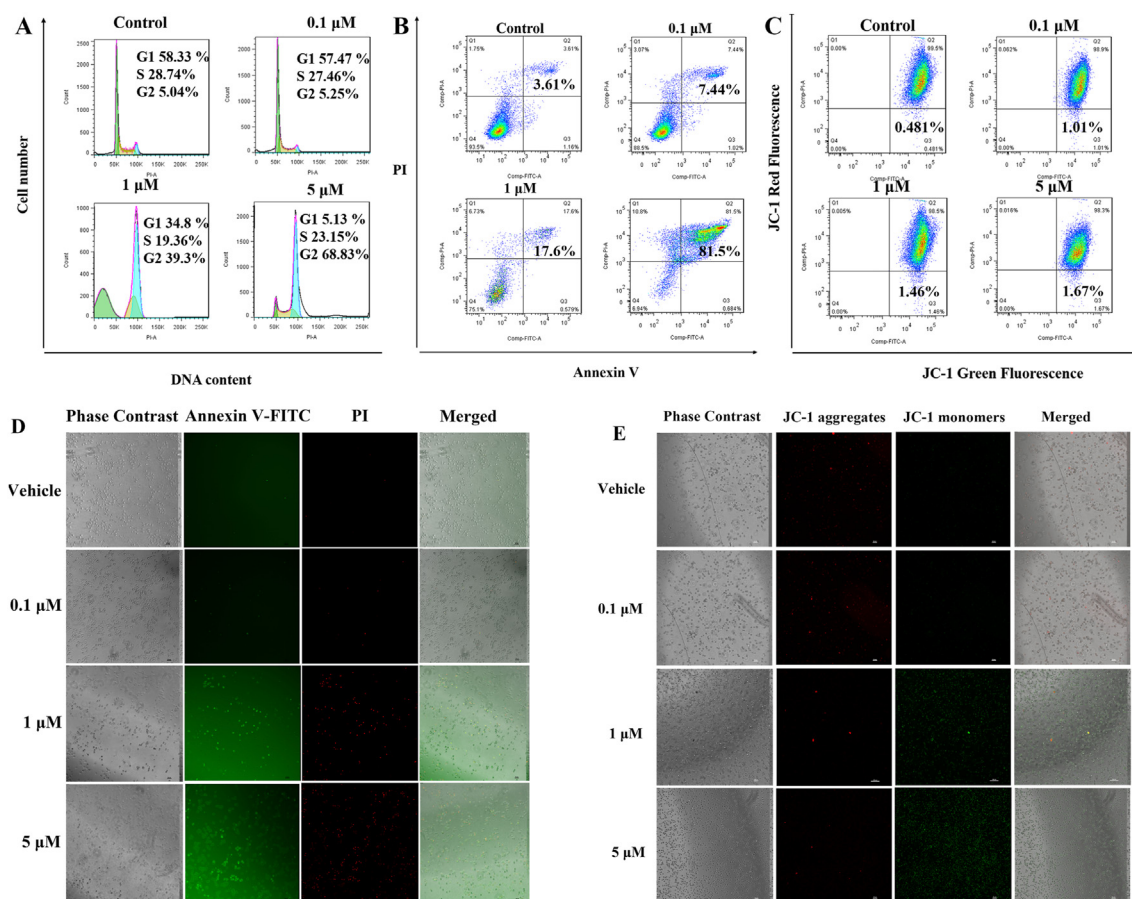


**Fig. 5.** HepG2 cells incubated with TP5 for 24 h were analyzed for cell cycle, apoptosis, and  $\Delta\Psi_m$  profiles. Flow cytometric analysis of: (A) cell cycle; (B) Annexin-FITC apoptosis; (C)  $\Delta\Psi_m$ ; and Fluorescence analysis of: (D) Annexin-FITC apoptosis; (E)  $\Delta\Psi_m$ .

of TP5. Based on the high *in vitro* antiproliferative activity, the similar binding affinities to human and murine PD-L1, and our continued interest in melanoma [12], TP5 was selected to evaluate the *in vivo* antitumor efficacy using a melanoma B16-F10 tumor model in humanized PD-1 C57BL/6J-*Pdcd1*<sup>em1(hPDCD1)/Smoc</sup> mice. As exhibited in Fig. 7, TP5 showed significant antitumor activity (Fig. 7A and B) and

stable body weight (Fig. 7C) during treatment. At the dose of 100 mg/kg via intragastric gavage, TP5 decreased the tumor weight and tumor volume by 57.9% and 82.8% respectively, as compared to vehicle control. One-way ANOVA analysis gave a *P* value of >0.05, suggesting no significant difference in the weight of spleen and thymus in the human PD-1 knock-in mice (Fig. 7D and E).

**Table 2**  
In vitro anti-PD-1/PD-L1 activities of CA-4 analogs.

ID	IC <sub>50</sub> (μM)	ID	IC <sub>50</sub> (μM)	ID	IC <sub>50</sub> (μM)
TP1	>100	TP9	>100	TP17	>100
TP2	44.79 ± 4.4	TP10	>100	TP18	38.57 ± 2.9
TP3	90.55 ± 8.6	TP11	42.05 ± 3.6	TP19	58.57 ± 4.3
TP4	>100	TP12	52.01 ± 7.1	TP20	>100
TP5	48.76 ± 3.8	TP13	>100	CA-4	>100
TP6	65.66 ± 7.6	TP14	89.99 ± 9.3	BMS-202	61.07 nM
TP7	>100	TP15	>100		
TP8	50.75 ± 6.1	TP16	>100		

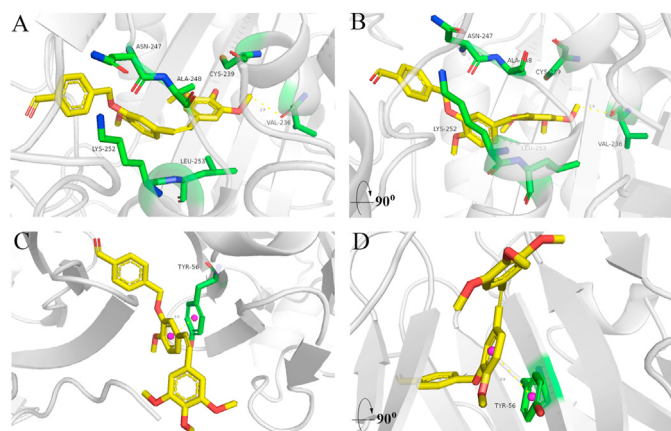


**Fig. 6.** Binding interactions between compound TP5 and target proteins (tubulin and PD-L1): (A) Docking analysis of compound TP5 in the colchicine binding of tubulin (PDB: 5H70); (B) 90° clockwise rotation of tubulin in complex with TP5 along x axis; (C) Docking analysis of compound TP5 in the hydrophobic cleft formed by the dimeric PD-L1 (PDB: 5J89); (D) 90° clockwise rotation of the dimeric PD-L1 in complex with TP5 along x axis.

Analysis of chemokines and tumor-infiltrating lymphocytes (TILs). To investigate the effects of TP5 in immune regulation, we first measured the relative mRNA levels of CXCR3, CXCL9, CXCL10, and PD-L1 in melanoma tumor tissues, because clinical research has demonstrated that intratumoral activity of chemokines (e.g. CXCR3, CXCL9, and CXCL10) is required for the efficacy of anti-PD-1/PD-L1 therapy, and the expression of PD-L1 is another key predictive marker for the response and outcome after treatment with PD-1/PD-L1 inhibitors [23,24]. As shown in Fig. 8, the mRNA expression levels of CXCR3 and CXCL10 but not CXCL9 were significantly increased in tumors (Fig. 8A, B, 8C). Furthermore, mRNA level of PD-L1 was significantly decreased upon TP5 treatment, as compared to vehicle control group (Fig. 8D). Clinical studies have shown that the PD-L1 levels decrease upon anti-PD-1/PD-L1 therapy with monoclonal antibodies, but the exact mechanism remains unclear [25–27]. Therefore, our results are in line with clinical studies in that the mRNA levels of PD-L1 decreased in the TP5-treated group.

Moreover, the percentages of helper T cells (CD3<sup>+</sup>CD4<sup>+</sup>) and

**Table 3**  
The binding affinity of TP5 to human or murine PD-L1 as measured by ITC and SPR.

ITC			SPR		
	hPD-L1	mPD-L1		hPD-L1	mPD-L1
K <sub>D</sub>	117 μM	75.4 μM	K <sub>D</sub>	49.5 μM	112 μM
ΔH	80	80	ka (1/Ms)	27.8	975
ΔG	-9.5	-9.7	kd (1/s)	1.38 × 10 <sup>-3</sup>	0.109
-TΔS	-89.5	-89.7	KA (1/M)	2.02 × 10 <sup>-4</sup>	8.91 × 10 <sup>-3</sup>

ΔG (enthalpy, kcal/mol), ΔH (entropy, kcal/mol), and -TΔS (free energy, kcal/mol).

activated cytotoxic T cells (CD3<sup>+</sup>CD8<sup>+</sup>) were significantly increased after treatment with TP5 but not in spleen, as compared to vehicle control group (Fig. 9A–F). Finally, the protein levels of PD-L1 were significantly decreased upon TP5 treatment, as compared to vehicle control group (Fig. 9G–J). Collectively, these data suggest that the antitumor activity of TP5 may be related to the activation of the tumor microenvironment.

*In vivo* safety analyses. To assess the *in vivo* safety profiles of TP5, we performed athohistological analysis utilizing haematoxylin-eosin (H&E) staining of kidney and liver collected at end of the *in vivo* study. As shown in Fig. 10A, no apparent morphological abnormalities in kidney and liver of different treatment groups was observed. In addition, serum biochemistry studies indicated that TP5 had no obvious nephrotoxicity and hepatotoxicity in human PD-1 knockin mice compared to the control group (Fig. 10B), as determined by the indicator levels of kidney and liver function (albumin/globulin (A/G); albumin (ALB); alanine aminotransferase (ALT); aminotransferase (AST); creatinine (CRE); blood urea nitrogen (UREA); aspartate globulin (GLO); total protein (TP) et al.).

Furthermore, the *in vivo* cardiotoxicity of TP5 was determined in BALB/c mice at doses of 100 mg/kg via intragastric gavage. During the 14 days of treatment, no apparent adverse effects were observed in BALB/c mice. Importantly, TP5 did not cause cardiotoxicity based on the electrocardiograms (ECG) (Fig. 11A and B). Moreover, auto hematology analysis revealed that TP5 had no myelosuppression as the lymphocyte, granulocyte and other routine hematological indicators were not significantly changed compared to control group (Fig. 11C). The above results suggest that TP5 has a benign *in vivo* safety profile.

### 3. Conclusions

In summary, novel CA-4 analogs based on PD-1/PD-L1 inhibitor and CA-4 were synthesized as dual inhibitors of tubulin and PD-1/PD-L1. Among them, compound TP5 showed strongest inhibitory effects against five cancer cell lines with an IC<sub>50</sub> value of 0.8 μM in HepG2 cells and negligible cytotoxicity to normal cells (IC<sub>50</sub> > 40 μM for HEK-293 and NCM460). In addition, mechanism of action studies suggest that TP5 exerted its effects by inhibiting tubulin polymerization, suppressing HepG2 cell migration and colony formation, causing cell arrest at G2/M phase, and inducing apoptosis. Furthermore, TP5 exhibited moderate anti-PD-1/PD-L1 activity with IC<sub>50</sub> values of 48.76 μM. *In vivo* efficacy studies indicated that TP5 could significantly suppress tumor growth in an immune checkpoint humanized mouse model with a Tumor Growth Suppression (TGI) of 57.9% at 100 mg/kg without causing significant toxicity. Moreover, TP5 did not cause *in vivo* cardiotoxicity and myelosuppression in BALB/c mice. These results suggest that the novel CA-4 analogs may serve as a starting point for developing more potent dual inhibitors of tubulin polymerization and PD-1/PD-L1.

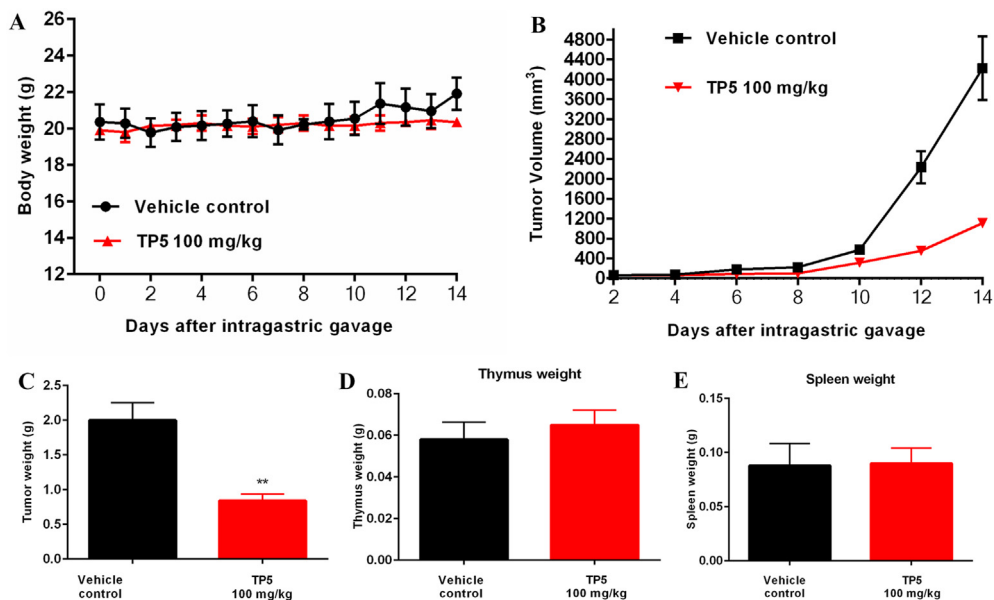


**Fig. 7.** Therapeutic effects of TP5 on human PD-1 knockin tumor mouse model. (A) Body weight changes; (B) Tumor volume; (C) Tumor weight; (D) Thymus weight; (E) Spleen weight. (\*\* $P < 0.05$  vs Vehicle control,  $n = 5$ , One-way ANOVA analysis).

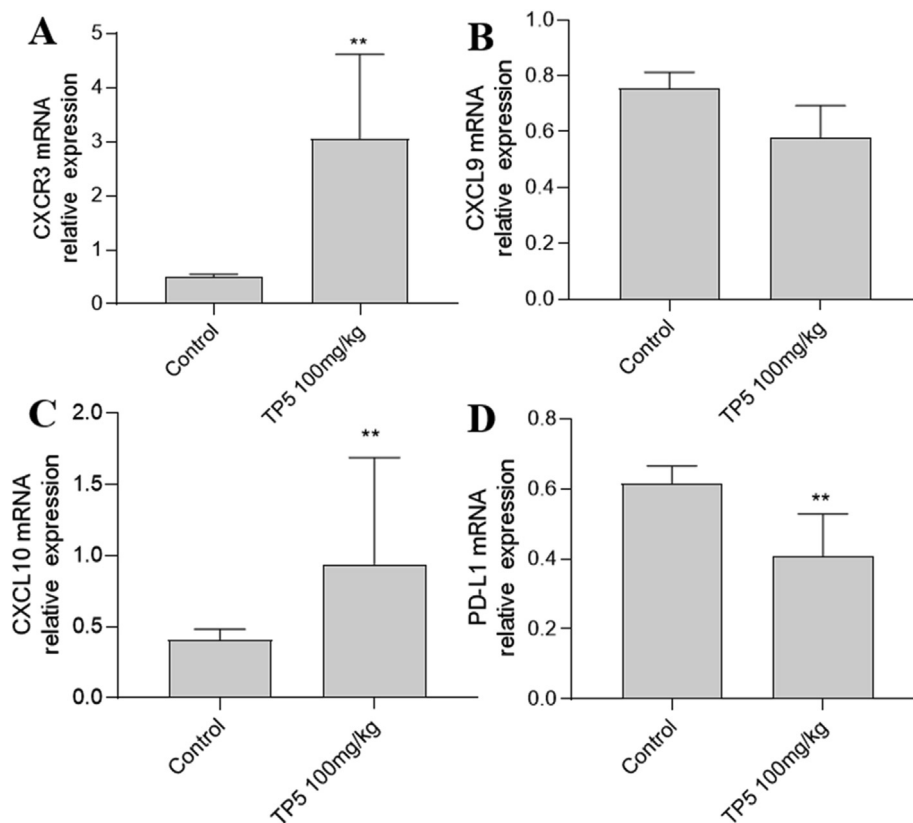


**Fig. 8.** Quantitative RT-PCR analysis of the mRNA expression for CXCR3, CXCL9, CXCL10, and PD-L1 in melanoma tumors. Relative expression of: (A) CXCR3 mRNA; (B) CXCL9 mRNA; (C) CXCL10 mRNA; (D) PD-L1 mRNA.

#### 4. Experimental section

**General methods.** Reagents and solvents were obtained from commercial sources and used without further purification. CA-4 was purchased from InvivoChem (Libertyville, IL 60048, USA) and

BMS-202 was purchased from Targetmol. All the reactions were monitored by TLC using silica gel GF/UV 254. All melting points were measured using a X-5 micro melting point apparatus. Flash chromatography was performed using silica gel (300–400 mesh). The <sup>1</sup>H and <sup>13</sup>C NMR spectra were recorded on Bruker AV-400

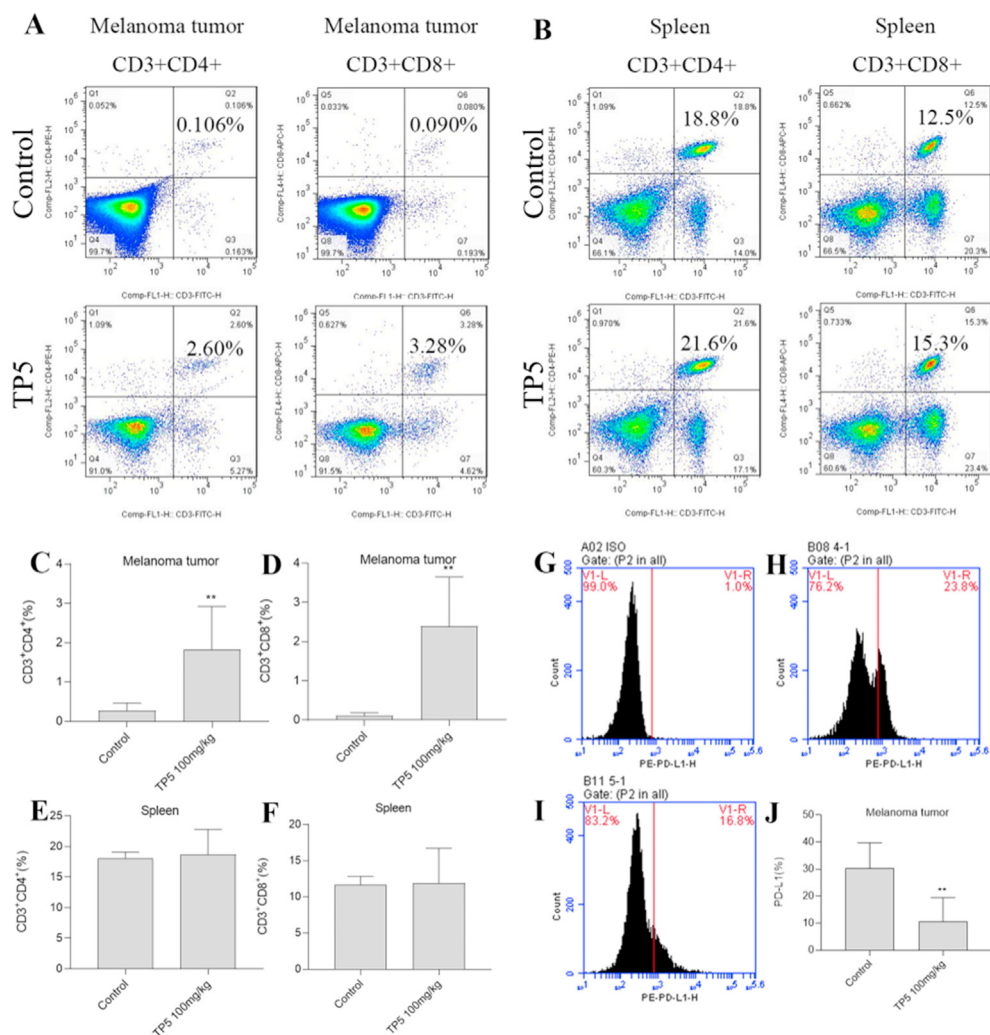


**Fig. 9.** (A) Representative examples for melanoma tumor helper T cells and activated cytotoxic T cells in control or TP5 treated mice; (B) Representative image for spleen helper T cells and activated cytotoxic T cells in control or TP5 treated; (C) Helper T cells in melanoma tumors (n = 5); (D) Activated cytotoxic T cells in melanoma tumors (n = 5); (E) Spleen helper T cells (n = 5); (F) Spleen activated cytotoxic T cells (n = 5); The expression levels of PD-L1 protein in melanoma tumors: (G) ISO control, (H) vehicle control, (I) TP5 treated, (J) Melanoma tumor PD-L1  $\pm$  SD (n = 5).

spectrometer, with TMS as an internal standard. High resolution mass spectrometry data (HRMS) were obtained using an Orbitrap Fusion™ Tribrid™ mass spectrometer (Thermo Scientific). Purity of all tested compounds was  $\geq 95\%$ , as estimated by HPLC (SHIMADZU LC-20A, UV detection at 254 nm) analysis on the C18 column ( $4.6 \times 150$  mm,  $5 \mu\text{m}$ ). HPLC conditions: flow rate, 1 mL/min with a mobile phase of water/MeOH; 60/40 water/MeOH was initially held for 1 min followed by a linear gradient from 60/40 to 5/95 water/MeOH over 15 min which was then held for 10 min.

**General method A:** To a solution of aryl benzyl alcohol in THF was added tribromoborane drop-wise at  $0^\circ\text{C}$ . TLC showed the reaction was completed. The reaction was quenched by MeOH slowly and then concentrated under reduced pressure to give a residue. The residue was purified by silica gel column chromatography using a gradient from 0% to 20% of Ethyl acetate in Petroleum ether to yield the desired compound.

**General method B:** A mixture of intermediates M1 (1.0 equiv),  $\text{Na}_2\text{CO}_3$  (1.5 equiv), CA-4 (1.5 equiv) in DMF (0.2 M) was stirred at  $80^\circ\text{C}$  for 30 min. TLC (Petroleum ether/Ethyl acetate = 2:1, Rf = 0.3) showed the starting material was consumed completely. The reaction mixture was poured into  $\text{H}_2\text{O}$  (10 mL), then the mixture was extracted with ethyl acetate (15 mL\*3). The organic phase was

washed with brine (10 mL\*2), dried over anhydrous  $\text{Na}_2\text{SO}_4$ , concentrated in vacuum to give a residue, which was further purified by silica gel column chromatography give desired compounds as white solid.

**General method C:** A solution of aromatic aldehyde compound (1.0 equiv), M3 (3.0 equiv), sodium cyanoborohydride (2.0 equiv), and AcOH (2 drops) in DMF (0.2 M) was stirred at  $80^\circ\text{C}$  for 1 h. The mixture was concentrated under reduce pressure. Purification by Prep-TLC provided the desired compounds.

## 5. Synthesis of compounds TP1–20

(Z)-1-(4-((2-methoxy-5-(3,4,5-trimethoxystyryl)phenoxy)methyl)benzyl)piperidine-2-carboxylic acid (TP1). The title compound was obtained as light yellow solid (3.9 mg, 15% yield); mp:  $166.9\text{--}168.2^\circ\text{C}$ ;  $^1\text{H}$  NMR (400 MHz, DMSO)  $\delta$  7.32 (d,  $J = 8.1$  Hz, 2H), 7.27 (d,  $J = 8.0$  Hz, 2H), 6.97–6.91 (m, 2H), 6.87 (dd,  $J = 8.4, 1.5$  Hz, 1H), 6.56 (s, 2H), 6.52–6.44 (m, 2H), 4.83 (s, 2H), 3.86 (d,  $J = 13.4$  Hz, 1H), 3.75 (s, 3H), 3.63 (d,  $J = 2.5$  Hz, 9H), 3.50 (d,  $J = 14.0$  Hz, 1H), 3.08 (dd,  $J = 7.6, 4.0$  Hz, 1H), 2.88–2.83 (m, 1H), 2.25–2.19 (m, 1H), 1.79 (d,  $J = 4.4$  Hz, 1H), 1.71 (dd,  $J = 8.2, 3.3$  Hz, 1H), 1.48 (d,  $J = 3.9$  Hz, 3H), 1.37 (d,  $J = 4.1$  Hz, 1H);  $^{13}\text{C}$  NMR (101 MHz, DMSO)

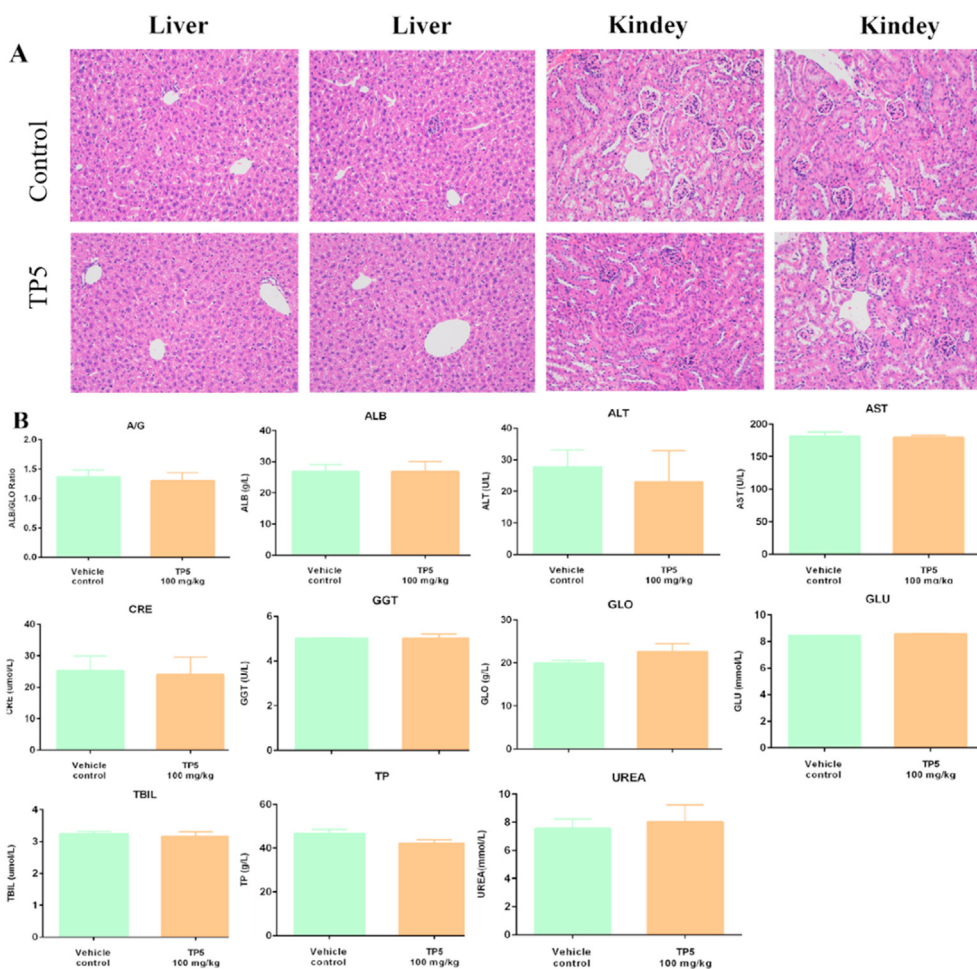


**Fig. 10.** (A) Pathological sections of kidney and liver obtained from human PD-1 knock-in mice; (B) Serum biochemistry analysis of indicator levels of kidney and liver function (A/G, ALB, ALT, AST, CRE, GGT, GLO, GLU, TBIL, TP, and UREA) in human PD-1 knock-in mice.

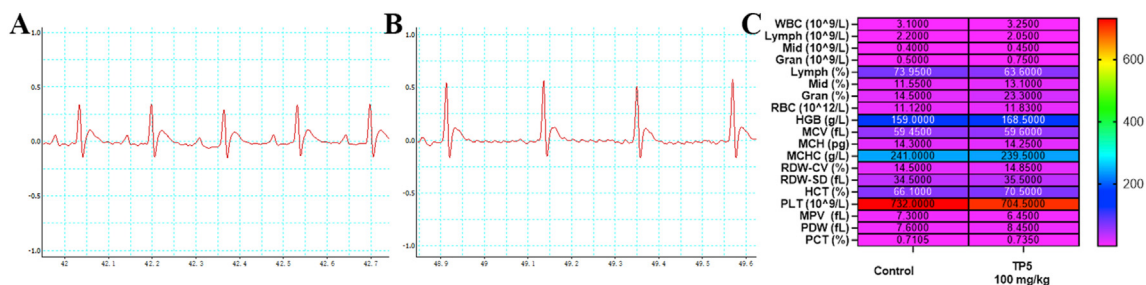


**Fig. 11.** Evaluation of *in vivo* cardiotoxicity and myelosuppression of TP5 by ECG and blood cell analysis in BALB/c mice. (A) Control (0.9% Saline) group; (B) TP5 100 mg/kg; (C) Auto hematology analysis.

$\delta$  173.83, 153.07, 148.92, 147.71, 137.10, 137.05, 136.41, 132.96, 129.81, 129.72, 129.00, 128.01, 122.45, 114.29, 112.27, 106.35, 70.14, 60.45, 59.07, 56.44, 56.07, 55.96, 49.55, 28.95, 24.59, 22.29; HRMS *m/z* calcd for C<sub>32</sub>H<sub>38</sub>O<sub>7</sub>N 548.2643, found 548.2637 [M + H<sup>+</sup>]; HPLC: *t*<sub>R</sub> 15.677 min, purity 95.223%.

(Z)-N-(2-((4-(2-methoxy-5-(3,4,5-trimethoxystyryl)phenoxy)methyl)benzyl)amino)ethyl)acetamide (TP2). The title compound was obtained as light yellow oil (4.1 mg, 16% yield); <sup>1</sup>H NMR (400 MHz, CDCl<sub>3</sub>)  $\delta$  7.28 (m, 4H), 6.88 (d, *J* = 1.5 Hz, 2H), 6.81 (d, *J* = 8.7 Hz, 1H), 6.45 (dd, *J* = 21.8, 10.8 Hz, 4H), 6.22 (m, 1H), 4.94 (s, 2H), 3.88 (s, 3H), 3.84 (s, 3H), 3.79 (s, 2H), 3.69 (s, 6H), 3.38 (dd,

*J* = 11.2, 5.5 Hz, 2H), 2.81 (t, *J* = 5.7 Hz, 2H), 2.19 (s, 1H), 1.99 (s, 3H); <sup>13</sup>C NMR (101 MHz, DMSO)  $\delta$  169.66, 167.82, 161.96, 153.08, 148.97, 147.46, 144.30, 139.94, 137.10, 136.04, 132.87, 130.04, 129.69, 129.14, 128.42, 127.95, 122.58, 114.60, 112.42, 106.31, 69.75, 60.46, 56.04, 42.72, 41.76, 22.96; HRMS *m/z* calcd for C<sub>30</sub>H<sub>37</sub>O<sub>6</sub>N<sub>2</sub> 521.2646, found 521.2657 [M + H<sup>+</sup>]; HPLC: *t*<sub>R</sub> 16.622 min, purity 96.564%.

(Z)-2-((4-(2-methoxy-5-(3,4,5-trimethoxystyryl)phenoxy)methyl)benzyl)amino)ethan-1-ol (TP3). The title compound was obtained as yellow oil (2.1 mg, 16.8% yield); <sup>1</sup>H NMR (400 MHz, DMSO)  $\delta$  7.30 (d, *J* = 8.0 Hz, 2H), 7.24 (d, *J* = 7.9 Hz, 2H), 6.91 (d, *J* = 8.3 Hz, 2H), 6.86 (dd, *J* = 8.5, 1.4 Hz, 1H), 6.56 (s, 2H), 6.48 (m,

2H), 5.33 (s, 1H), 4.81 (s, 2H), 4.48 (s, 1H), 3.74 (s, 3H), 3.70 (s, 2H), 3.63 (s, 9H), 3.46 (m, 2H), 2.56 (t,  $J = 5.8$  Hz, 2H);  $^{13}\text{C}$  NMR (101 MHz, DMSO)  $\delta$  153.17, 148.90, 148.24, 147.62, 133.01, 132.99, 130.33, 130.07, 129.83, 129.57, 128.97, 128.40, 127.96, 114.20, 112.26, 106.34, 70.14, 60.64, 60.40, 56.08, 55.96, 52.96, 51.23; HRMS  $m/z$  calcd for  $\text{C}_{28}\text{H}_{34}\text{O}_6\text{N}$  480.2381, found 480.2387 [ $\text{M} + \text{H}^+$ ]; HPLC:  $t_{\text{R}}$  15.180 min, purity 95.576%.

(Z)-2-((4-((2-methoxy-5-(3,4,5-trimethoxystyryl)phenoxy)methyl)benzyl)amino)-2-methylpropanoic acid (TP4). The title compound was obtained as white solid (5.6 mg, 18% yield); mp: 200.5–201.3 °C;  $^1\text{H}$  NMR (400 MHz, DMSO)  $\delta$  7.44 (d,  $J = 8.0$  Hz, 2H), 7.31 (d,  $J = 8.0$  Hz, 2H), 6.92 (dd,  $J = 4.9, 3.3$  Hz, 2H), 6.87 (dd,  $J = 8.5, 1.4$  Hz, 1H), 6.56 (s, 2H), 6.47 (d,  $J = 2.3$  Hz, 2H), 5.33 (s, 1H), 4.86 (s, 2H), 3.89 (s, 2H), 3.75 (s, 3H), 3.63 (s, 9H), 1.33 (s, 6H);  $^{13}\text{C}$  NMR (101 MHz, DMSO)  $\delta$  188.00, 170.82, 152.91, 148.79, 147.12, 144.23, 136.80, 135.84, 133.04, 130.08, 129.70, 129.62, 129.07, 127.78, 122.96, 114.25, 112.34, 106.15, 69.67, 60.55, 57.05, 55.96, 24.37; HRMS  $m/z$  calcd for  $\text{C}_{30}\text{H}_{36}\text{O}_7\text{N}$  522.2486, found 522.2482 [ $\text{M} + \text{H}^+$ ]; HPLC:  $t_{\text{R}}$  15.567 min, purity 95.020%.

(Z)-4-((2-methoxy-5-(3,4,5-trimethoxystyryl)phenoxy)methyl)benzaldehyde (TP5). The title compound was obtained as yellow oil (500 mg, 60% yield);  $^1\text{H}$  NMR (400 MHz, DMSO)  $\delta$  10.00 (s, 1H), 7.89 (d,  $J = 8.0$  Hz, 2H), 7.52 (d,  $J = 8.0$  Hz, 2H), 6.94 (d,  $J = 8.2$  Hz, 1H), 6.88 (dd,  $J = 10.1, 1.8$  Hz, 2H), 6.53 (s, 2H), 6.50–6.43 (m, 2H), 5.01 (s, 2H), 3.77 (s, 3H), 3.62 (d,  $J = 14.0$  Hz, 9H);  $^{13}\text{C}$  NMR (101 MHz, DMSO)  $\delta$  193.13, 153.04, 148.97, 147.46, 144.29, 137.09, 136.03, 132.86, 130.04, 129.68, 129.13, 127.94, 122.69, 114.59, 112.42, 106.31, 69.74, 60.45, 56.03; HRMS  $m/z$  calcd for  $\text{C}_{26}\text{H}_{27}\text{O}$  435.1802, found 435.1800 [ $\text{M} + \text{H}^+$ ]; HPLC:  $t_{\text{R}}$  17.963 min, purity 96.065%.

(Z)-N-(2-aminoethyl)-1-(4-((2-methoxy-5-(3,4,5-trimethoxystyryl)phenoxy)methyl)benzyl)piperidine-2-carboxamide (TP6). The title compound was obtained as yellow oil (2 mg, 15% yield);  $^1\text{H}$  NMR (400 MHz,  $\text{CDCl}_3$ )  $\delta$  7.47 (d,  $J = 7.9$  Hz, 1H), 7.38 (d,  $J = 8.1$  Hz, 1H), 7.10 (d,  $J = 8.5$  Hz, 0H), 6.91 (m, 1H), 6.81 (d,  $J = 8.2$  Hz, 0H), 6.73 (s, 1H), 6.53 (s, 1H), 6.47 (q,  $J = 12.1$  Hz, 2H), 4.90 (s, 1H), 3.93 (s, 1H), 3.92 (s, 1H), 3.88 (d,  $J = 3.8$  Hz, 1H), 3.84 (s, 1H), 3.72 (s, 3H), 3.48 (s, 1H), 3.33 (d,  $J = 9.1$  Hz, 1H), 2.95 (s, 1H), 2.03 (s, 1H), 1.73 (d,  $J = 7.1$  Hz, 1H), 1.62 (m, 1H), 1.48 (d,  $J = 9.3$  Hz, 1H);  $^{13}\text{C}$  NMR (101 MHz, DMSO)  $\delta$  168.46, 152.93, 148.79, 147.34, 136.94, 134.60, 132.97, 132.12, 130.19, 130.03, 129.73, 129.52, 128.99, 127.97, 122.63, 114.27, 112.21, 106.26, 69.75, 65.64, 60.25, 56.06, 56.00, 40.15, 28.94, 28.79, 28.48; HRMS  $m/z$  calcd for  $\text{C}_{34}\text{H}_{44}\text{O}_6\text{N}_3$  590.3225, found 590.3228 [ $\text{M} + \text{H}^+$ ]; HPLC:  $t_{\text{R}}$  16.407 min, purity 95.660%.

*tert*-butyl (Z)-2-(1-(4-((2-methoxy-5-(3,4,5-trimethoxystyryl)phenoxy)methyl)benzyl)piperidine-2-carboxamido)ethyl)carbamate (TP7). The title compound was obtained as yellow oil (20 mg, 25% yield);  $^1\text{H}$  NMR (400 MHz, DMSO)  $\delta$  7.81 (t,  $J = 5.6$  Hz, 1H), 7.33 (d,  $J = 7.8$  Hz, 2H), 7.26 (d,  $J = 8.0$  Hz, 2H), 6.92 (d,  $J = 8.1$  Hz, 2H), 6.87 (dd,  $J = 6.2, 2.0$  Hz, 1H), 6.77 (t,  $J = 5.3$  Hz, 1H), 6.56 (s, 2H), 6.48 (m, 2H), 4.83 (s, 2H), 3.75 (s, 3H), 3.70 (d,  $J = 13.3$  Hz, 1H), 3.63 (d,  $J = 2.4$  Hz, 9H), 3.16 (dd,  $J = 12.3, 6.7$  Hz, 2H), 3.08 (d,  $J = 13.2$  Hz, 1H), 3.00 (m, 2H), 2.70 (s, 1H), 2.67 (s, 1H), 2.00 (m, 1H), 1.87 (t,  $J = 10.8$  Hz, 1H), 1.73 (dd,  $J = 12.5, 2.4$  Hz, 1H), 1.63 (dd,  $J = 11.6, 4.2$  Hz, 1H), 1.51 (m, 3H), 1.34 (s, 9H);  $^{13}\text{C}$  NMR (101 MHz, DMSO)  $\delta$  173.86, 158.60, 156.08, 153.07, 148.92, 147.72, 137.10, 132.96, 130.06, 129.82, 129.59, 129.45, 129.00, 127.86, 122.41, 114.26, 112.27, 106.35, 78.06, 70.13, 60.45, 56.07, 55.96, 28.55, 26.94, 25.50, 22.49; HRMS  $m/z$  calcd for  $\text{C}_{39}\text{H}_{52}\text{O}_8\text{N}_3$  690.3749, found 690.3754 [ $\text{M} + \text{H}^+$ ]; HPLC:  $t_{\text{R}}$  19.400 min, purity 97.254%.

(4-((2-methoxy-5-((Z)-3,4,5-trimethoxystyryl)phenoxy)methyl)benzyl)-L-threonine (TP8). The title compound was obtained as white solid (4.2 mg, 19% yield); mp: 137.4–138.6 °C;  $^1\text{H}$  NMR (400 MHz, DMSO)  $\delta$  7.36 (d,  $J = 6.9$  Hz, 2H), 7.28 (d,  $J = 8.0$  Hz, 2H), 7.20 (s, 1H), 6.92 (d,  $J = 8.3$  Hz, 2H), 6.87 (dd,  $J = 8.6, 1.1$  Hz, 1H),

6.65 (s, 1H), 6.56 (s, 2H), 6.49 (m, 2H), 5.33 (s, 1H), 4.84 (s, 2H), 3.93 (m, 1H), 3.85 (d,  $J = 6.7$  Hz, 1H), 3.75 (s, 3H), 3.65 (m, 9H), 3.52 (s, 2H), 1.09 (d,  $J = 6.3$  Hz, 3H);  $^{13}\text{C}$  NMR (101 MHz, DMSO)  $\delta$  176.55, 153.17, 147.45, 146.37, 130.00, 129.80, 129.50, 128.35, 127.57, 106.36, 106.36, 99.82, 72.49, 72.02, 70.64, 61.69, 56.09, 55.97, 22.24; HRMS  $m/z$  calcd for  $\text{C}_{30}\text{H}_{36}\text{O}_8\text{N}$  538.2435, found 538.2435 [ $\text{M} + \text{H}^+$ ]; HPLC:  $t_{\text{R}}$  15.352 min, purity 96.274%.

(2R,4R)-4-hydroxy-1-(4-((2-methoxy-5-((Z)-3,4,5-trimethoxystyryl)phenoxy)methyl)benzyl)pyrrolidine-2-carboxylic acid (TP9). The title compound was obtained as white solid (3.2 mg, 15% yield); mp: 140.9–142.1 °C;  $^1\text{H}$  NMR (400 MHz, DMSO)  $\delta$  7.31 (dd,  $J = 20.1, 7.1$  Hz, 4H), 7.19 (s, 1H), 6.92 (d,  $J = 8.2$  Hz, 2H), 6.87 (dd,  $J = 8.3, 1.4$  Hz, 1H), 6.56 (s, 2H), 6.48 (q,  $J = 11.8$  Hz, 2H), 5.33 (s, 1H), 4.83 (s, 2H), 4.18 (s, 1H), 4.02 (d,  $J = 11.9$  Hz, 1H), 3.75 (s, 3H), 3.63 (s, 9H), 3.52 (s, 2H), 1.99 (s, 2H), 1.46 (dd,  $J = 7.5, 5.0$  Hz, 2H);  $^{13}\text{C}$  NMR (101 MHz, DMSO)  $\delta$  171.46, 159.96, 159.39, 158.59, 152.91, 147.12, 144.23, 136.80, 135.84, 133.05, 130.09, 129.71, 129.07, 127.78, 122.97, 114.25, 112.34, 106.15, 69.67, 68.84, 60.55, 59.65, 55.96, 52.61, 37.41; HRMS  $m/z$  calcd for  $\text{C}_{31}\text{H}_{36}\text{O}_8\text{N}$  550.2435, found 550.2432 [ $\text{M} + \text{H}^+$ ]; HPLC:  $t_{\text{R}}$  15.080 min, purity 95.268%.

(Z)-4-((2-methoxy-5-(3,4,5-trimethoxystyryl)phenoxy)methyl)phenyl)methanol (TP10). The title compound was obtained as white solid (6 mg, 23% yield); mp: 60.2–61.3 °C;  $^1\text{H}$  NMR (400 MHz, DMSO)  $\delta$  7.43 (d,  $J = 8.0$  Hz, 2H), 7.35 (d,  $J = 8.1$  Hz, 2H), 6.93 (d,  $J = 8.3$  Hz, 2H), 6.88 (d,  $J = 8.1$  Hz, 1H), 6.56 (s, 2H), 6.48 (q,  $J = 12.2$  Hz, 2H), 4.88 (s, 2H), 4.10 (s, 2H), 3.76 (s, 3H), 3.63 (d,  $J = 4.4$  Hz, 9H);  $^{13}\text{C}$  NMR (101 MHz, DMSO)  $\delta$  153.09, 148.93, 147.70, 142.68, 137.10, 135.59, 132.98, 129.83, 129.56, 128.96, 127.85, 126.84, 122.42, 114.26, 112.28, 106.35, 70.16, 63.04, 60.45, 56.08, 55.97; HRMS  $m/z$  calcd for  $\text{C}_{26}\text{H}_{27}\text{O}_6$  435.1813, found 435.1806 [ $\text{M} - \text{H}^+$ ]; HPLC:  $t_{\text{R}}$  15.086 min, purity 95.253%.

(Z)-1-(4-((2-methoxy-5-(3,4,5-trimethoxystyryl)phenoxy)methyl)benzyl)azetidine-3-carboxylic acid (TP11). The title compound was obtained as white solid (3.1 mg, 15.2% yield); mp: 139.6–140.9 °C;  $^1\text{H}$  NMR (400 MHz, DMSO)  $\delta$  7.24 (s, 4H), 6.92 (d,  $J = 8.3$  Hz, 2H), 6.86 (d,  $J = 10.1$  Hz, 1H), 6.56 (s, 2H), 6.48 (d,  $J = 4.3$  Hz, 2H), 5.33 (m, 1H), 4.81 (s, 2H), 3.74 (s, 3H), 3.63 (d,  $J = 2.6$  Hz, 9H), 3.52 (d,  $J = 3.8$  Hz, 4H), 3.17 (d,  $J = 1.2$  Hz, 3H);  $^{13}\text{C}$  NMR (101 MHz, DMSO)  $\delta$  173.33, 152.91, 148.80, 147.12, 141.16, 136.80, 135.84, 133.04, 130.08, 129.70, 129.62, 129.07, 127.77, 122.96, 114.24, 112.34, 106.15, 69.66, 60.54, 55.96, 49.41, 37.17; HRMS  $m/z$  calcd for  $\text{C}_{30}\text{H}_{34}\text{O}_7\text{N}$  520.2330, found 520.2324 [ $\text{M} + \text{H}^+$ ]; HPLC:  $t_{\text{R}}$  15.103 min, purity 95.899%.

(3S,4S)-4-fluoro-1-(4-((2-methoxy-5-((Z)-3,4,5-trimethoxystyryl)phenoxy)methyl)benzyl)pyrrolidin-3-ol (TP12). The title compound was obtained as yellow oil (6.5 mg, 23% yield);  $^1\text{H}$  NMR (400 MHz, DMSO)  $\delta$  7.27 (m, 4H), 6.92 (d,  $J = 8.6$  Hz, 2H), 6.87 (d,  $J = 8.3$  Hz, 1H), 6.56 (s, 2H), 6.48 (m, 2H), 5.31 (d,  $J = 4.7$  Hz, 1H), 4.81 (m, 3H), 4.16 (dd,  $J = 24.2, 5.4$  Hz, 1H), 3.75 (s, 3H), 3.57 (m, 11H), 3.03 (dd,  $J = 9.4, 6.7$  Hz, 1H), 2.68 (m, 2H), 2.16 (d,  $J = 15.1$  Hz, 1H);  $^{13}\text{C}$  NMR (101 MHz, DMSO)  $\delta$  153.08, 148.92, 147.72, 137.10, 132.97, 129.81, 129.59, 128.99, 128.01, 122.44, 114.29, 112.27, 106.35, 75.57, 75.32, 70.16, 60.45, 59.25, 58.23, 56.07, 55.96; HRMS  $m/z$  calcd for  $\text{C}_{30}\text{H}_{35}\text{O}_6\text{NF}$  524.2443, found 524.2455 [ $\text{M} + \text{H}^+$ ]; HPLC:  $t_{\text{R}}$  17.533 min, purity 98.363%.

(R,Z)-1-(4-((2-methoxy-5-(3,4,5-trimethoxystyryl)phenoxy)methyl)benzyl)pyrrolidin-3-ol (TP13). The title compound was obtained as yellow oil (5 mg, 19% yield);  $^1\text{H}$  NMR (400 MHz, DMSO)  $\delta$  7.27 (q,  $J = 8.1$  Hz, 4H), 6.92 (d,  $J = 8.4$  Hz, 2H), 6.86 (dd,  $J = 8.3, 1.5$  Hz, 1H), 6.56 (s, 2H), 6.48 (m, 2H), 4.82 (s, 2H), 4.68 (s, 1H), 4.17 (s, 1H), 3.75 (s, 3H), 3.57 (m, 11H), 2.68 (t,  $J = 6.9$  Hz, 1H), 2.58 (d,  $J = 0.8$  Hz, 1H), 2.40 (s, 1H), 2.29 (s, 1H), 1.99 (m, 1H), 1.54 (d,  $J = 7.9$  Hz, 1H);  $^{13}\text{C}$  NMR (101 MHz, DMSO)  $\delta$  153.08, 148.92, 147.74, 137.11, 135.72, 132.96, 129.82, 129.59, 128.99, 128.92, 127.96, 122.41, 114.27, 112.27, 106.36, 70.18, 69.79, 62.96, 60.45, 59.79, 56.07, 55.96,

52.77, 34.74; HRMS  $m/z$  calcd for  $C_{30}H_{36}O_6N$  506.2537, found 506.2534  $[M + H^+]$ ; HPLC:  $t_R$  16.587 min, purity 98.799%.

(S,Z)-1-(4-((2-methoxy-5-(3,4,5-trimethoxystyryl)phenoxy)methyl)benzyl)pyrrolidin-3-ol (TP14). The title compound was obtained as yellow oil (4.8 mg, 18% yield);  $^1H$  NMR (400 MHz, DMSO)  $\delta$  7.29 (dd,  $J = 20.0, 7.9$  Hz, 4H), 6.92 (m, 2H), 6.86 (dd,  $J = 8.3, 1.5$  Hz, 1H), 6.56 (s, 2H), 6.48 (m, 2H), 4.82 (d,  $J = 10.0$  Hz, 3H), 4.22 (s, 1H), 3.74 (s, 3H), 3.64 (m, 12H), 2.73 (m, 2H), 2.39 (s, 1H), 2.01 (m, 1H), 1.58 (s, 1H);  $^{13}C$  NMR (101 MHz, DMSO)  $\delta$  153.03, 148.84, 147.55, 138.95, 136.97, 135.70, 133.06, 129.82, 129.55, 129.10, 128.96, 127.92, 122.56, 114.09, 112.21, 106.28, 99.93, 70.10, 69.73, 60.49, 59.67, 56.04, 55.91, 52.62, 34.40; HRMS  $m/z$  calcd for  $C_{30}H_{36}O_6N$  506.2537, found 506.2538  $[M + H^+]$ ; HPLC:  $t_R$  16.770 min, purity 95.844%.

(R,Z)-1-(4-((2-methoxy-5-(3,4,5-trimethoxystyryl)phenoxy)methyl)benzyl)pyrrolidine-3-carboxylic acid (TP15). The title compound was obtained as light yellow solid (3.1 mg, 15% yield); mp: 156.3–157.8 °C;  $^1H$  NMR (400 MHz, DMSO)  $\delta$  7.26 (q,  $J = 8.2$  Hz, 4H), 6.92 (d,  $J = 8.2$  Hz, 2H), 6.86 (dd,  $J = 8.2, 1.5$  Hz, 1H), 6.56 (s, 2H), 6.48 (q,  $J = 12.3$  Hz, 2H), 4.83 (s, 2H), 3.75 (s, 3H), 3.63 (d,  $J = 2.4$  Hz, 9H), 3.56 (d,  $J = 5.1$  Hz, 3H), 2.91 (d,  $J = 7.6$  Hz, 1H), 2.69 (t,  $J = 8.7$  Hz, 1H), 2.59 (m, 1H), 2.45 (s, 1H), 1.96 (d,  $J = 7.3$  Hz, 2H);  $^{13}C$  NMR (101 MHz, DMSO)  $\delta$  174.90, 152.89, 148.92, 147.66, 137.06, 135.83, 135.43, 129.98, 129.82, 129.59, 128.94, 127.91, 122.46, 114.29, 106.27, 70.16, 60.36, 59.19, 56.59, 56.07, 55.93, 53.48, 26.87; HRMS  $m/z$  calcd for  $C_{31}H_{36}O_7N$  548.2643, found 548.2641  $[M + H^+]$ ; HPLC:  $t_R$  15.104 min, purity 96.839%.

(R,Z)-1-(4-((2-methoxy-5-(3,4,5-trimethoxystyryl)phenoxy)methyl)benzyl)piperidine-2-carboxylic acid (TP16). The title compound was obtained as yellow solid (4.2 mg, 17% yield); mp: 170.1–171.3 °C;  $^1H$  NMR (400 MHz, DMSO)  $\delta$  7.32 (d,  $J = 8.1$  Hz, 2H), 7.27 (d,  $J = 8.0$  Hz, 2H), 6.92 (d,  $J = 9.1$  Hz, 2H), 6.87 (d,  $J = 8.3$  Hz, 1H), 6.56 (s, 2H), 6.48 (q,  $J = 12.2$  Hz, 2H), 4.83 (s, 2H), 3.87 (d,  $J = 13.3$  Hz, 1H), 3.75 (s, 3H), 3.63 (d,  $J = 2.3$  Hz, 9H), 3.51 (s, 1H), 3.07 (m, 1H), 2.86 (dd,  $J = 12.5, 4.3$  Hz, 1H), 2.20 (m, 1H), 2.01 (dd,  $J = 14.7, 7.0$  Hz, 1H), 1.81 (d,  $J = 12.9$  Hz, 1H), 1.70 (m, 1H), 1.48 (dd,  $J = 16.8, 10.8$  Hz, 3H), 1.35 (d,  $J = 6.4$  Hz, 1H);  $^{13}C$  NMR (101 MHz, DMSO)  $\delta$  164.04, 152.88, 149.09, 147.44, 137.04, 136.49, 132.94, 129.86, 129.51, 129.00, 127.94, 122.46, 114.31, 112.27, 106.22, 70.13, 64.54, 60.56, 59.03, 56.22, 55.74, 48.82, 29.07, 24.36, 22.24; HRMS  $m/z$  calcd for  $C_{32}H_{38}O_7N$  548.2643, found 548.2641  $[M + H^+]$ ; HPLC:  $t_R$  15.540 min, purity 95.035%.

(S,Z)-1-(4-((2-methoxy-5-(3,4,5-trimethoxystyryl)phenoxy)methyl)benzyl)piperidine-2-carboxylic acid (TP17). The title compound was obtained as yellow solid (5.2 mg, 16% yield); mp: 167.3–168.9 °C;  $^1H$  NMR (400 MHz, DMSO)  $\delta$  7.33 (d,  $J = 8.0$  Hz, 2H), 7.27 (d,  $J = 8.0$  Hz, 2H), 6.92 (d,  $J = 8.7$  Hz, 2H), 6.87 (m, 1H), 6.56 (s, 2H), 6.48 (m, 2H), 4.83 (s, 2H), 3.88 (d,  $J = 13.3$  Hz, 1H), 3.75 (s, 3H), 3.63 (d,  $J = 2.5$  Hz, 9H), 3.53 (s, 1H), 3.07 (d,  $J = 3.8$  Hz, 1H), 2.86 (m, 1H), 2.22 (dd,  $J = 12.1, 7.2$  Hz, 1H), 1.99 (t,  $J = 6.4$  Hz, 1H), 1.81 (dd,  $J = 10.1, 6.3$  Hz, 1H), 1.70 (dd,  $J = 12.4, 4.0$  Hz, 1H), 1.49 (dd,  $J = 20.7, 14.3$  Hz, 3H), 1.34 (m, 1H);  $^{13}C$  NMR (101 MHz, DMSO)  $\delta$  167.32, 154.11, 152.94, 147.91, 132.78, 131.83, 129.81, 129.52, 127.78, 122.22, 116.15, 112.21, 106.39, 69.85, 60.35, 56.24, 55.95, 29.36, 25.63, 23.24; HRMS  $m/z$  calcd for  $C_{32}H_{38}O_7N$  548.2643, found 548.2645  $[M + H^+]$ ; HPLC:  $t_R$  15.543 min, purity 95.002%.

(S,Z)-1-(4-((2-methoxy-5-(3,4,5-trimethoxystyryl)phenoxy)methyl)benzyl)pyrrolidine-3-carboxylic acid (TP18). The title compound was obtained as yellow solid (4.6 mg, 17% yield); mp: 157.6–158.9 °C;  $^1H$  NMR (400 MHz, DMSO)  $\delta$  7.27 (q,  $J = 8.1$  Hz, 4H), 6.92 (d,  $J = 8.1$  Hz, 2H), 6.86 (dd,  $J = 8.4, 1.4$  Hz, 1H), 6.56 (s, 2H), 6.48 (m, 2H), 4.83 (s, 2H), 3.75 (s, 3H), 3.63 (d,  $J = 2.5$  Hz, 9H), 3.57 (d,  $J = 4.7$  Hz, 3H), 2.92 (m, 1H), 2.70 (t,  $J = 8.8$  Hz, 1H), 2.61 (d,  $J = 6.6$  Hz, 1H), 2.48 (s, 1H), 1.95 (dd,  $J = 14.5, 7.4$  Hz, 2H);  $^{13}C$  NMR (101 MHz, DMSO)  $\delta$  176.19, 153.07, 148.92, 147.72, 137.10, 135.87,

132.97, 129.82, 129.59, 128.96, 127.98, 122.43, 114.29, 112.27, 106.35, 70.16, 60.45, 59.17, 56.55, 56.07, 55.96, 53.62, 41.86, 27.49; HRMS  $m/z$  calcd for  $C_{31}H_{36}O_7N$  534.2486, found 534.2489  $[M + H^+]$ ; HPLC:  $t_R$  15.108 min, purity 96.136%.

(4-((2-methoxy-5-((Z)-3,4,5-trimethoxystyryl)phenoxy)methyl)benzyl)-L-allothreonine (TP19). The title compound was obtained as white solid (2.3 mg, 15% yield); mp: 137.8–138.9 °C;  $^1H$  NMR (400 MHz, DMSO)  $\delta$  7.37 (d,  $J = 7.8$  Hz, 2H), 7.28 (d,  $J = 8.0$  Hz, 2H), 7.19 (s, 1H), 6.92 (d,  $J = 8.3$  Hz, 2H), 6.86 (dd,  $J = 8.4, 1.4$  Hz, 1H), 6.65 (s, 1H), 6.56 (s, 2H), 6.48 (m, 2H), 5.33 (s, 1H), 4.84 (s, 2H), 3.96 (d,  $J = 16.0$  Hz, 1H), 3.83 (m, 1H), 3.75 (s, 3H), 3.63 (d,  $J = 2.1$  Hz, 9H), 2.92 (d,  $J = 2.8$  Hz, 2H), 1.10 (d,  $J = 6.3$  Hz, 3H);  $^{13}C$  NMR (101 MHz, DMSO)  $\delta$  174.13, 153.15, 147.49, 147.42, 136.95, 135.73, 133.19, 130.02, 129.76, 128.73, 127.95, 113.99, 112.15, 106.29, 70.92, 70.14, 60.35, 55.68, 54.33, 24.16; HRMS  $m/z$  calcd for  $C_{30}H_{36}O_8N$  534.2435, found 538.2437  $[M + H^+]$ ; HPLC:  $t_R$  15.324 min, purity 100%.

(Z)-N<sup>1</sup>-(4-((2-methoxy-5-(3,4,5-trimethoxystyryl)phenoxy)methyl)benzyl)-N<sub>2</sub>,N<sub>2</sub>-dimethylethane-1,2-diamine (TP20). The title compound was obtained as colorless oil (2.3 mg, 15% yield);  $^1H$  NMR (400 MHz, DMSO)  $\delta$  7.26 (m, 4H), 6.92 (d,  $J = 8.3$  Hz, 2H), 6.86 (dd,  $J = 8.3, 1.6$  Hz, 1H), 6.56 (s, 2H), 6.48 (m, 2H), 4.83 (s, 2H), 3.75 (s, 3H), 3.63 (d,  $J = 2.7$  Hz, 9H), 3.39 (s, 2H), 2.51 (m, 4H), 2.14 (s, 6H);  $^{13}C$  NMR (101 MHz, DMSO)  $\delta$  153.07, 148.92, 147.72, 137.09, 135.90, 132.96, 129.81, 129.59, 129.21, 129.00, 127.95, 122.43, 114.29, 112.27, 106.35, 70.17, 63.42, 60.45, 56.06, 55.96, 45.28; HRMS  $m/z$  calcd for  $C_{30}H_{39}O_5N_2$  507.2859, found 507.2860  $[M + H^+]$ ; HPLC:  $t_R$  17.754 min, purity 95.593%.

*In vitro* PD-1/PD-L1 (HTRF) binding assay. The ability of the newly synthesized compounds in inhibition of PD-1/PD-L1 interaction were performed using a PD-1/PD-L1 HTRF binding assay. The PD-1/PD-L1 binding assay kits (Cisbio, Cat. no. 64ICP01-PEG&64ICP01PEH) were purchased from Cisbio. The experiments were performed according to the manufacturer's guidelines.

*In vitro* antiproliferative assay. The cytotoxicity of the synthesized compounds was determined using the CCK-8 assay. Briefly, the cell lines were incubated at 37 °C in a humidified 5% CO<sub>2</sub> incubator for 24 h in 96-microwell plates. Then, 100  $\mu$ L of culture medium with 0.1% DMSO containing the test compounds at different concentrations was added to each well and incubated at 37 °C for another 48 h. The optical density was detected with a microplate reader at 450 nm. The IC<sub>50</sub> values were calculated according to the dose-dependent curves.

*In vitro* tubulin polymerization assay. Pig brain microtubule protein was isolated via three cycles of temperature-dependent assembly/disassembly in 100 mM PIPES (pH 6.5), 1 mM GTP, 1 mM MgSO<sub>4</sub>, 2 mM EGTA and 1 mM 2-mercaptoethanol. Glycerol and phenylmethylsulfonyl fluoride were added to 4 M and 0.2 mM in the first cycle of polymerization. Tubulin was prepared from microtubule protein by phosphocellulose (P11) chromatography, stored at –70 °C. Tubulin was mixed with different concentrations of compound in PEM buffer (100 mM PIPES, 1 mM MgCl<sub>2</sub>, and 1 mM EGTA) containing 1 mM GTP and 5% glycerol. Microtubule polymerization was detected by a spectrophotometer at 340 nm at 37 °C. The plateau absorbance values were used for calculations.

Colony formation assay. HepG2 cells (1000 units) were counted and seeded in 6-well plates. After cultured for 24 h at 37 °C, the medium was replaced with medium added with compound TP5 at the indicated concentration. After 24 h treatment, the medium was changed to normal. Cultured for another 7–10 days, the colonies were fixed with 4% paraformaldehyde for 30 min and stained with 0.1% Crystal Violet for 15 min. Following washed with PBS, the colonies were then photographed and quantified using Image J.

Annexin V-FITC/propidium iodide (PI) apoptosis detection. HepG2 cells were grown in 6-well plates and incubated overnight. After exposure to TP5 for 24 h, cells were harvested and washed

twice with PBS. The apoptosis rate was analyzed by flow cytometry with FITC Annexin V/PI apoptosis detection kit following the manufacturer's instructions.

Mitochondrial membrane potential ( $\Delta\Psi_m$ ) determination. HepG2 Cells were plated in 6-well plates overnight, then treated with TP5 for 24 h. Mitochondrial membrane potential was assessed by flow cytometry using a JC-1 mitochondrial membrane potential detection kit according to the protocol.

Cell-cycle analysis. HepG2 cells were seeded in 6-well plates and then exposed to TP5 for 24 h. After that, cells were harvested by trypsinization, washed in cold PBS and fixed in ice-cold 70% ethanol overnight at  $-20^\circ\text{C}$ . The cell cycle was detected using a cell cycle analysis kit by flow cytometry.

Wound healing assay. HepG2 cell migration was evaluated by scratch wound healing assay. When HepG2 cells were grown to full confluence in six-well plates and wounded linearly by a pipette tip. The remaining cells were rinsed with PBS. Cells were incubated with TP5. Photographs of wound closure were taken at 0 h and 24 h.

Confocal imaging of tubulin polymerization. HepG2 cells were plated on glass coverslips, 24 h later cells were treated with TP5 for 24 h. After washed in PBS, cells were fixed for 15 min with 4% formaldehyde prior to permeabilization in 0.2% Triton X-100 for 5 min, and blocked with 5% BSA for 30 min. Then, cells were immunostained with anti-tubulin antibody and FITC-conjugated anti-CREST antibody, and confocal laser scanning was carried out with Zeiss710 confocal imaging system.

ITC and SPR analysis. All the proteins were obtained from Sino Biological if not otherwise specified: human PD-L1 (Cat No:10084-HNAH), murine PD-L1 (Cat No:50010-M08H). SPRi measurements were performed with PlexArray HT (Plexera Bioscience, Seattle, WA, USA). Briefly, human/murine PD-L1 were diluted to a final concentration of 0.25 mg/mL with sterile water and printed onto the bare gold-coated PlexArray Nanocapture Sensor Chip, then compound TP5 was injected by a nonpulsatile piston pump into the 30  $\mu\text{L}$  flow cell, which was mounted on the coupling prim. The ITC experiment was performed using a MicroCal PEAQ-ITC (Malvern Panalytical Ltd., UK), ITC experiments were performed according to the manufacturer's guidelines.

Immune checkpoint humanized mouse models. On the C57BL/6 background, the full-length coding sequence of human PDCD-1 gene was placed immediately downstream of the start codon of the mouse endogenous *Pdcd1*, followed by a poly(A) element. This guarantees an exclusive expression of human PD-1 in the humanized PD-1 mice (Shanghai Model Organisms Center, Inc.). The animal protocols were approved by the National Institutional Animal Care and ethical Committee of Southern Medical University. B16F10 cells growing in a logarithmic growth phase were suspended in PBS at a density of  $1 \times 10^6$  per mL. Each mouse was inoculated subcutaneously with 200  $\mu\text{L}$  containing  $2 \times 10^5$  cells. After tumors reached approximately 50  $\text{mm}^3$  in volume, mice were randomly divided into three groups ( $n = 5$ ) and treated with compound TP5 (100 mg/kg) and vehicle respectively. Compound TP5 was formulated in 30% PEG-300 and 70% saline. The drugs were administered via intragastric gavage once a day for 14 days. Animal activity and body weight were monitored during the entire experiment period to assess acute toxicity. Two weeks later, mice were sacrificed and the tumor tissue, major organs (liver, spleen, thymus and kidney) samples were collected. The harvested tumor tissue and organs (liver, kidney) were fixed in 4% paraformaldehyde, processed into paraffin routinely, stained with haematoxylin and eosin (H&E) and captured by microscope. Tumor Growth Inhibition value (TGI) was calculated using the formula:  $\text{TGI} (\%) = [1 - \text{Wt}/\text{Wv}] * 100\%$ , where Wt and Wv are the mean tumor weight of treatment group and vehicle control.

Flow cytometry. Organs of mice were harvested and cells were

isolated by mechanical dissociation using 40  $\mu\text{m}$  cell strainers. Red blood cells were lysed by ACK lysis buffer (Beyotime). Cells were stained for 30 min at  $4^\circ\text{C}$  for flow cytometry using antibodies against following targets and isotype controls, both obtained from BioLegend if not otherwise specified: FITC anti-mouse CD3 Antibody (Cat No:100204, LOT: B249620), APC anti-mouse CD8a Antibody (Cat No:100711, LOT:B280032), PE anti-mouse CD4 Antibody (Cat No:100407, LOT:B266389), Anti-mouse-PD-L1-PE Antibody (Cat#:124307, Lot:B284420), Rat IgG2b K Isotype Control PE (Cat#:400608, Lot:B156144). Flow cytometry for murine cells was performed on a BD AccuriC6 and data was analyzed using FlowJo (Tree Star v7.6.1).

qPCR analysis of the mRNA expression for CXCR3, CXCL9, CXCL10, and PD-L1 in melanoma tumors. Primer sequences for the detection of CXCL9 were 5'-TCTGGCTTCCAGAGCCACAC-3' and 5'-TCTAGCTCACCAGCAAACAGACA-3', for CXCR3 were 5'-GCCAAGC-CATGTACCTTGAG-3' and 5'-TCAGGCTGAAATCCTGTGG-3', for CD274 were 5'-TGGCAGGAGAGGAGGACCTT-3' and 5'-TGT AGTCCGCACCACCGTAG-3', and for CXCL10 were 5'-GAGGGCCA-TAGGGAAGCTTGA-3' and 5'-GTGTGTGCGTGGCTTCACTC-3'. All samples were normalized using GAPDH detected using 5'-GGAAAGCTGTGGCGTGATGG-3' and 5'-AGTCTGGGATGACCTTGCC-3' primers.

*In vivo* cardiotoxicity by ECG and blood cell analysis. BALB/c mice from Liaoning Changsheng Biotechnology Co., Ltd., aged 6–8 weeks old, were used to study the cardiotoxicity of TP5. TP5 was administered via intragastric gavage once a day for 14 days. Instrument used: PowerLab (ADI Instruments Castle Hill, NSW, Australia). Electrodes were inserted into the right forelimb (cathode), left limb (anode) and right hind limb (ground) subcutaneously. The right hind limb serves as the reference electrode. The whole blood was also collected into a heparin sodium anticoagulation tube used for blood cell analysis.

Statistical analysis. Data was analyzed using Prism Software 5.0. Data was provided as mean  $\pm$  SD unless otherwise indicated. The statistical significance ( $P < 0.05$ ) was calculated by one-way analysis of variance (ANOVA).

Molecular docking. Molecular graphic manipulations and visualizations were performed using Glide 7.4. X-ray structures of PD-L1 and tubulin in complex with their respective ligands were retrieved from the PDB (5H70 and 5J89).

## Associated content

### Supporting information

$^1\text{H}$  NMR,  $^{13}\text{C}$  NMR, HRMS, and HPLC spectra.

### Notes

The authors declare no competing financial interest.

## Declaration of competing interest

The authors declare that they have no known competing financial interests or personal relationships that could have appeared to influence the work reported in this paper.

## Acknowledgments

This work was supported by scientific research project of high level talents (No. C1051008) in Southern Medical University of China; and International Science and Technology Cooperation Projects of Guangdong Province (No. G819310411).

## References

- [1] E.S. Soteriades, J. Kim, C.A. Christophi, S.N. Kales, Cancer incidence and mortality in firefighters: a state-of-the-art review and meta-analysis, *Asian Pac. J. Cancer Prev. APJCP* 20 (2019) 3221–3231.
- [2] C. Demoor-Goldschmidt, F. de Vathaire, Review of risk factors of secondary cancers among cancer survivors, *Br. J. Radiol.* 92 (2019) 20180390.
- [3] A. Anighoro, J. Bajorath, G. Rastelli, Polypharmacology: challenges and opportunities in drug discovery, *J. Med. Chem.* 57 (2014) 7874–7887.
- [4] N.M. Raghavendra, D. Pingili, S. Kadasi, A. Mettu, S. Prasad, Dual or multi-targeting inhibitors: the next generation anticancer agents, *Eur. J. Med. Chem.* 143 (2018) 1277–1300.
- [5] X.T. Christian Bailly, Quesnel Bruno, Combined cytotoxic chemotherapy and immunotherapy of cancer: modern times, *NAR Cancer* 2 (2020) 20.
- [6] C. Hardin, E. Shum, A.P. Singh, R. Perez-Soler, H. Cheng, Emerging treatment using tubulin inhibitors in advanced non-small cell lung cancer, *Expert Opin. Pharmacother.* 18 (2017) 701–716.
- [7] H. Hayashi, K. Nakagawa, Combination therapy with PD-1 or PD-L1 inhibitors for cancer, *Int. J. Clin. Oncol.* 25 (2020) 818–830.
- [8] D.B. Page, H. Bear, S. Prabhakaran, M.E. Gatti-Mays, A. Thomas, E. Cobain, H. McArthur, J.M. Balko, S.R. Gameiro, R. Nanda, J.L. Gulley, K. Kalinsky, J. White, J. Litton, S.J. Chmura, M.Y. Polley, B. Vincent, D.W. Cescon, M.L. Disis, J.A. Sparano, E.A. Mittendorf, S. Adams, Two may be better than one: PD-1/PD-L1 blockade combination approaches in metastatic breast cancer, *NPJ Breast Cancer* 5 (2019) 34.
- [9] G. Li, Y. Wang, L. Li, Y. Ren, X. Deng, J. Liu, W. Wang, M. Luo, S. Liu, J. Chen, Design, synthesis, and bioevaluation of pyrazolo[1,5-a]pyrimidine derivatives as tubulin polymerization inhibitors targeting the colchicine binding site with potent anticancer activities, *Eur. J. Med. Chem.* 202 (2020) 112519.
- [10] L. Li, D. Quan, J. Chen, J. Ding, J. Zhao, L. Lv, J. Chen, Design, synthesis, and biological evaluation of 1-substituted -2-aryl imidazoles targeting tubulin polymerization as potential anticancer agents, *Eur. J. Med. Chem.* 184 (2019) 111732.
- [11] B. Cheng, Y. Ren, H. Cao, J. Chen, Discovery of novel resorcinol diphenyl ether-based PROTAC-like molecules as dual inhibitors and degraders of PD-L1, *Eur. J. Med. Chem.* 199 (2020) 112377.
- [12] B. Cheng, Y. Ren, X. Niu, W. Wang, S. Wang, Y. Tu, S. Liu, J. Wang, D. Yang, G. Liao, J. Chen, Discovery of novel resorcinol dibenzyl ethers targeting the programmed cell death-1/programmed cell death-ligand 1 interaction as potential anticancer agents, *J. Med. Chem.* 63 (2020) 8338–8358.
- [13] E. Pasquier, M. Kavallaris, Microtubules: a dynamic target in cancer therapy, *IUBMB Life* 60 (2008) 165–170.
- [14] C.H. Shen, J.J. Shee, J.Y. Wu, Y.W. Lin, J.D. Wu, Y.W. Liu, Combretastatin A-4 inhibits cell growth and metastasis in bladder cancer cells and retards tumour growth in a murine orthotopic bladder tumour model, *Br. J. Pharmacol.* 160 (2010) 2008–2027.
- [15] A. Siebert, M. Gensicka, G. Cholewinski, K. Dzierzbicka, Synthesis of Combretastatin A-4 analogs and their biological activities, *Anticancer Agents Med Chem* 16 (2016) 942–960.
- [16] R.J. Sullivan, K.T. Flaherty, Immunotherapy: anti-PD-1 therapies—a new first-line option in advanced melanoma, *Nat. Rev. Clin. Oncol.* 12 (2015) 625–626.
- [17] B. Cheng, W.E. Yuan, J. Su, Y. Liu, J. Chen, Recent advances in small molecule based cancer immunotherapy, *Eur. J. Med. Chem.* 157 (2018) 582–598.
- [18] P.G. Sasikumar, M. Ramachandra, Small-molecule immune checkpoint inhibitors targeting PD-1/PD-L1 and other emerging checkpoint pathways, *BioDrugs* 32 (2018) 481–497.
- [19] S. Shaabani, H.P.S. Huizinga, R. Butera, A. Kouchi, K. Guzik, K. Magiera-Mularz, T.A. Holak, A. Domling, A patent review on PD-1/PD-L1 antagonists: small molecules, peptides, and macrocycles (2015–2018), *Expert Opin. Ther. Pat.* 28 (2018) 665–678.
- [20] M. Qin, Q. Cao, X. Wu, C. Liu, S. Zheng, H. Xie, Y. Tian, J. Xie, Y. Zhao, Y. Hou, X. Zhang, B. Xu, H. Zhang, X. Wang, Discovery of the programmed cell death-1/programmed cell death-ligand 1 interaction inhibitors bearing an indoline scaffold, *Eur. J. Med. Chem.* 186 (2020) 111856.
- [21] M. Qin, Q. Cao, S. Zheng, Y. Tian, H. Zhang, J. Xie, H. Xie, Y. Liu, Y. Zhao, P. Gong, Discovery of [1,2,4]Triazol[4,3-*a*]pyridines as potent inhibitors targeting the programmed cell death-1/programmed cell death-ligand 1 interaction, *J. Med. Chem.* 62 (2019) 4703–4715.
- [22] K. Guzik, K.M. Zak, P. Grudnik, K. Magiera, B. Musielak, R. Torner, L. Skalniak, A. Domling, G. Dubin, T.A. Holak, Small-molecule inhibitors of the programmed cell death-1/programmed cell death-ligand 1 (PD-1/PD-L1) interaction via transiently induced protein states and dimerization of PD-L1, *J. Med. Chem.* 60 (2017) 5857–5867.
- [23] M.T. Chow, A.J. Ozga, R.L. Servis, D.T. Frederick, J.A. Lo, D.E. Fisher, G.J. Freeman, G.M. Boland, A.D. Luster, Intratumoral activity of the CXCR3 chemokine system is required for the efficacy of anti-PD-1 therapy, *Immunity* 50 (2019) 1498–1512, e1495.
- [24] V.R. Juneja, K.A. McGuire, R.T. Manguso, M.W. LaFleur, N. Collins, W.N. Haining, G.J. Freeman, A.H. Sharpe, PD-L1 on tumor cells is sufficient for immune evasion in immunogenic tumors and inhibits CD8 T cell cytotoxicity, *J. Exp. Med.* 214 (2017) 895–904.
- [25] X. Frigola, B.A. Inman, C.M. Lohse, C.J. Krco, J.C. Cheville, R.H. Thompson, B. Leibovich, M.L. Blute, H. Dong, E.D. Kwon, Identification of a soluble form of B7-H1 that retains immunosuppressive activity and is associated with aggressive renal cell carcinoma, *Clin. Canc. Res.* 17 (2011) 1915–1923.
- [26] T. Nagato, T. Ohkuri, K. Ohara, Y. Hirata, K. Kishibe, Y. Komabayashi, S. Ueda, M. Takahara, T. Kumai, K. Ishibashi, A. Kosaka, N. Aoki, K. Oikawa, Y. Uno, N. Akiyama, M. Sado, H. Takei, E. Celis, Y. Harabuchi, H. Kobayashi, Programmed death-ligand 1 and its soluble form are highly expressed in nasal natural killer/T-cell lymphoma: a potential rationale for immunotherapy, *Cancer Immunol. Immunother.* 66 (2017) 877–890.
- [27] D. Rossille, M. Gressier, D. Damotte, D. Maucort-Boulch, C. Pangault, G. Semana, S. Le Gouill, C. Haioun, K. Tarte, T. Lamy, N. Milpied, T. Fest, S. Groupe Ouest-Est des Leucemies et Autres Maladies du, S. Groupe Ouest-Est des Leucemies et Autres Maladies du, High level of soluble programmed cell death ligand 1 in blood impacts overall survival in aggressive diffuse large B-Cell lymphoma: results from a French multicenter clinical trial, *Leukemia* 28 (2014) 2367–2375.